Physical-Layer Security of RIS-Assisted Networks Over Correlated Fisher-Snedecor $\mathcal{F}$ Fading Channels

Saeid Pakravan, Jean-Yves Chouinard, *Life Senior Member, IEEE*, Ming Zeng, *Member, IEEE*, Xingwang Li, *Senior Member, IEEE*, Wanming Hao, *Senior Member, IEEE*, and Octavia A. Dobre, *Fellow, IEEE*

***Abstract*—This article investigates the performance of physical-layer security (PLS) in wireless communication systems, where a reconfigurable intelligent surfaces (RISs) is deployed between the transmitter and legitimate receiver to enhance the communication security. The Fisher-Snedecor $\mathcal{F}$ distribution is adopted to model the underlying fading channels, owing to its accuracy, tractability and generality. On this basis, this article evaluates the performance of the proposed system by deriving the average secrecy capacity (ASC) and the secrecy outage probability (SOP) under correlated Fisher-Snedecor $\mathcal{F}$ channel coefficients. Furthermore, the asymptotic behavior of the ASC and SOP in the high-signal-to-noise ratio (SNR) regime is examined. Analyzing the correlated scenario is crucial as it provides a detailed understanding of how interdependencies among channel coefficients impact the system's security and overall performance, offering valuable insights into real-world communication scenarios. Finally, this article verifies the analytical results through numerical illustrations, and demonstrates the effectiveness of employing RIS.**

***Index Terms*—Average secrecy capacity (ASC), correlated Fisher-Snedecor $\mathcal{F}$ fading channels, physical-layer security (PLS), reconfigurable intelligent surface (RIS), secrecy outage probability (SOP).**

I. Introduction

RECENTLY, reconfigurable intelligent surfaces (RISs) have emerged as a viable and economical approach to enhance the reliability and performance of future wireless communication systems [1]. RISs are artificial surfaces composed of electromagnetic material with numerous passive reflecting elements, enabling intelligent control over the wireless propagation environment and improvement in the quality of received signals. However, the exponential increase in the utilization of wireless intelligent devices, coupled with the broadcast nature of wireless channels, poses significant challenges in terms of security and privacy for designing next-generation wireless networks, including the sixth-generation (6-G) technology. A promising method to ensure secure communication and protect information from unauthorized access is through physical-layer security (PLS). PLS, often referred to as the classic wiretap channel [2], leverages the physical characteristics of the wireless propagation environment to enhance transmission security. Accurate modeling of the statistical characteristics of fading channel coefficients becomes crucial in this context.

In recent studies, the Fisher-Snedecor $\mathcal{F}$ distribution, also known as the $\mathcal{F}$-distribution, holds a significant position in statistical modeling due to its versatile applications across various fields [3], [4], [5]. Originating from the ratio of two chi-squared distributions, this distribution plays a crucial role in statistical hypothesis testing, regression analysis, and notably, in characterizing the behavior of random variables. Its emergence in diverse contexts, from economics to engineering, underscores its relevance as a fundamental probability distribution. In the domain of wireless communications, particularly in assessing fading phenomena and channel modeling, the Fisher-Snedecor distribution has gained traction for its ability to effectively capture complex signal behaviors, notably in scenarios involving shadowing and multipath fading. This distribution distinguishes itself through its superior capacity to model extreme values within the empirical cumulative density function (CDF) compared to the generalized-K model, notably evident in the intricate dynamics of composite fading scenarios. Consequently, this distribution proves itself as a practical and reliable tool for characterizing fading phenomena in wireless networks. Its notable capability to faithfully represent the occurrence of deep fading events, as evidenced by its alignment with the empirical CDF tail, highlights its applicability and credibility in this domain. A practical scenario where Fisher-Snedecor fading channels could be relevant is in urban or

This work was supported in part by the "Double First-Class" Discipline Creation Project of Surveying Science and Technology under Grant GCCRC202306, and in part by the Key Research and Development Project of Henan Province under Grant 231111210500. The work of Ming Zeng and Octavia A. Dobre was supported in part by the Natural Sciences and Engineering Research Council of Canada through its Discovery Program. *(Corresponding author: Saeid Pakravan.)*

Saeid Pakravan, Jean-Yves Chouinard, and Ming Zeng are with the Department of Electric and Computer Engineering, Laval University, Quebec City, QC G1V 0A6, Canada (e-mail: saeid.pakravan.1@ulaval.ca; Jean-Yves.Chouinard@gel.ulaval.ca; ming.zeng@gel.ulaval.ca).

Xingwang Li is with the School of Physics and Electronic Information Engineering, Henan Polytechnic University, Jiaozuo 454000, China, and also with Jiaozuo Key Laboratory of Crow-Sensing Network, Jiaozuo 454003, China (e-mail: lixingwang@hpu.edu.cn).

Wanming Hao is with the School of Electrical and Information Engineering, Zhengzhou University, Zhengzhou 450001, China (e-mail: iewmhao@zzu.edu.cn).

Octavia A. Dobre is with the Faculty of Engineering and Applied Science, Memorial University, St. John's, NL A1B 3X5, Canada (e-mail: odobre@mun.ca).

densely populated areas, where multipath propagation and signal scattering occur due to the presence of buildings, vehicles, and other obstacles [6]. In such environments, the received signal strength can fluctuate significantly due to the constructive and destructive interference patterns arising from the multipath components. The Fisher-Snedecor distribution could aptly characterize the statistical distribution of signal power fluctuations in these scenarios. Furthermore, wireless communication systems operating in non-line-of-sight (NLOS) conditions, such as indoor environments or within foliage, can also exhibit fading effects resembling those modeled by the Fisher-Snedecor distribution [7]. In NLOS situations, signals reach the receiver after undergoing multiple reflections and diffractions, leading to a complex composite channel that the Fisher-Snedecor distribution can capture effectively. Furthermore, in vehicular communication systems, especially those involving mobile users and rapidly changing environments, Fisher-Snedecor fading channels can simulate the varying channel conditions resulting from the movement of vehicles and the dynamic interference caused by other transmitters [8].

The Fisher-Snedecor $\mathcal{F}$ distribution is notable not only for its efficacy in portraying composite fading but also for its mathematical tractability. Its probability density function (PDF) of the Fisher-Snedecor $\mathcal{F}$ distribution comprises elementary functions with respect to the random variable (RV), thereby facilitating simpler analytical examinations in contrast to the intricate nature of the Generalized-K model. Furthermore, its versatility expands beyond its adeptness in capturing composite fading dynamics, as it showcases adaptability to transformations that facilitate seamless transitions into diverse established fading models used in various domains. This inherent flexibility and mathematical manageability position the Fisher-Snedecor $\mathcal{F}$ distribution as an appealing and robust choice for the analysis and modeling of fading characteristics in the context of wireless communication scenarios.

Recent research has extensively explored the role of RIS in PLS from different perspectives [9], [10]. Despite the increasing attention on RIS, there is a noticeable scarcity in research focusing on their role in safeguarding communications within fading channels [11], [12], [13], [14], [15], [16]. A study centers on analyzing the secrecy performance within RIS-aided wireless communication systems under Rayleigh fading channels [11], considering the scenario where the eavesdropper can also receive signals from the RIS. By deriving a closed-form expression for the secrecy outage probability (SOP), the authors demonstrate that the system without the RIS-eavesdropper link outperforms the system with the RIS utilized by the eavesdropper, indicating a degradation in secrecy performance when the eavesdropper exploits the advantages of RIS. Furthermore, the exploration of RIS-aided secure communication systems extends to different fading channels, specifically Nakagami-m and Fisher-Snedecor $\mathcal{F}$ fading channels as investigated in [12], [13], [14], [15], [16]. The investigation presented in [12] delves into Nakagami-m fading channels, presenting analytical expressions for the SOP and ergodic secrecy capacity. The authors meticulously unravel the intricacies of secure communication in the presence of RIS, shedding light on the performance metrics crucial for assessing system reliability. Likewise, the exploration in [13] centers around the Fisher-Snedecor $\mathcal{F}$ fading channels. The SOP and average secrecy capacity (ASC) are derived under the scenario where RIS is exclusively employed by the transmitter as an access point (AP). Notably, in this setup, there is an absence of RIS nodes between the transmitter and legitimate receiver. This specific configuration provides valuable insights into the impact of RIS in scenarios where the primary communication link involves only the transmitter and a dedicated RIS-based AP. Moving forward, [14] widens the scope by analyzing the SOP and ASC within cellular communications. Leveraging stochastic geometry theory, this study goes beyond the specific fading channels, employing a broader framework for analysis. The authors utilize this theory to generate PDFs and CDFs for the received signal-to-interference-plus-noise ratio (SINR) at each node. This approach allows for a comprehensive examination of the system's performance in cellular communication scenarios, providing a robust foundation for understanding the impact of RIS on the SINR distribution. References [15] and [16] address scenarios involving a legitimate transmitter, an authorized receiver, a RIS, and a passive eavesdropper. Both works assume that the fading channel coefficients follow an independent Fisher-Snedecor $\mathcal{F}$ distribution. Reference [15] establishes closed-form expressions for ASC and SOP, introducing a direct link between the source and the eavesdropper. Further, [16] provides closed-form expressions for ASC and SOP and also explores their asymptotic behavior. Notably, [16] features no direct link between the source and the eavesdropper; instead, the eavesdropper intercepts the message between the source and destination through a RIS, contributing a unique perspective to RIS-enabled secure communication.

However, it is crucial to emphasize the dependence among fading coefficients, a critical aspect often downplayed in the analysis of wireless communication theory for computational convenience. This correlation is highly influenced by factors, such as the proximity of transmitters, the presence or absence of scatters around the receivers, and the physical environments [17]. Therefore, the challenge in analyzing the performance of these correlated channels is how to generate multivariate distributions that represent the joint statistics of different fading coefficients. Being able to incorporate intricate dependence structures, copula theory appears to be a promising approach to address this challenge [18]. Copulas have been widely used in image processing, machine learning, and statistics [19]. In recent years, there has been gained popularity in the employment of dependence structures for the purpose of evaluating the performance of wireless communication systems. This development is underpinned by empirical data and motivated by the prospect of intelligently devising and controlling dependence structures to enhance system performance [20]. The application of copulas has been demonstrated in prior research endeavors to establish general bounds on the occurrence of outage performance in channels with correlated fading that has a slow time-varying nature [21]. Furthermore, copulas have been employed to investigate the PLS performance in a wiretap channel featuring correlated Rayleigh fading [22], [23]. Additionally, some other studies have

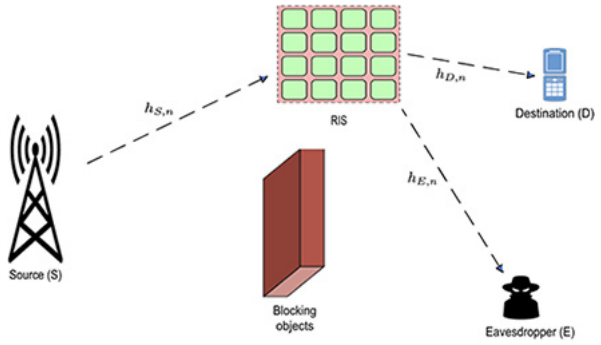

Fig. 1. System model for the considered network, with a source, a destination, an eavesdropper, and an RIS.

analyzed the impact of correlation between channel coefficient in multiuser fading channels [24], [25], [26], [27], [28]. These findings highlight the importance of considering dependence structures in wireless communication analysis and underscore the potential benefits of incorporating copula theory into performance analysis.

Motivated by the potential advancements that RIS and PLS technologies present in improving forthcoming wireless communication systems, the significant role played by the Fisher-Snedecor $\mathcal{F}$ distribution in accurately representing the combined influence of multipath fading and shadowing, as well as the correlated nature of fading in practical scenarios, this article focuses on the examination of a RIS-aided secure communication system over correlated Fisher-Snedecor $\mathcal{F}$ fading channels. The distinguishing aspect between our research and prior literature [9], [10], [11], [12], [13], [14], [15], [16] resides in the utilization of copula theory to examine the ramifications of channel correlation on the efficacy of secure communication systems employing RIS. In particular, we address the presence of correlated Fisher-Snedecor $\mathcal{F}$ distributions. This scholarly approach allows us to gain deeper insights into the intricacies of secure communication in the context of RIS-assisted systems and their vulnerability to correlated channel conditions and potential eavesdropping attacks.

In this context, to evaluate the impacts of RIS deployment and fading severity on the PLS performance, we present analytical expressions for the PDF and CDF of signal-to-noise ratios (SNRs). Then, we utilize the copula theory in combination with conventional statistical methods to evaluate the efficiency of the studied system model. This method offers a distinct advantage by enabling the examination of various dependence structures that exceed the constraints of linear dependence. To validate the accuracy of the analytical results, Monte-Carlo simulation results are presented and match very well with the theoretical ones, verifying the accuracy of the analysis. The findings demonstrate that the incorporation of RIS in secure communication systems leads to enhanced performance of secrecy metrics. In particular, the principal contributions can be succinctly outlined as:

1) We present the general expressions for the ASC and the SOP under correlated Fisher-Snedecor $\mathcal{F}$ fading channels, and analyze the asymptotic behavior of the ASC and SOP in the high-SNR regime.
2) We demonstrate how the analytical expression for the Farlie-Gumbel-Morgenstern (FGM) copula structure can be used to characterize the performances of the ASC and SOP.
3) Our analysis focuses on how the fading correlation affects the performance of considered system model. We analyze this performance particularly in terms of ASC and SOP, and do this by adjusting the copula dependence parameter within a certain range. Additionally, we investigate how the severity of fading affects the efficiency of the ASC and SOP.

This article is structured as follows: Section II presents the system model. Section III introduces the conceptual framework of copula, accompanied by the analytical formulations of ASC and SOP tailored for correlated system models. Section IV analyzes the asymptotic behavior of the obtained secrecy metrics in high SNR regime. Section V demonstrates numerically the effectiveness of the analytical results. Section VI draws conclusions.

Notation: Var(.) and $E(.)$ represent the variance and expectation operators, respectively. $[x]^+ = \max(x, 0)$ and $\text{Res}[f(x), p]$ is the residue of function $f(x)$ at pole $x = p$. The functions $\Gamma(.)$ and $\gamma(.,.)$ denote the complete and incomplete Gamma functions, respectively [29, eqs. (8.31)–(8.35)]. $B(.,.)$ represents the Beta function as defined in [29, eq. (8.38)]. ${}_2F_1(.,.;.;.)$ represents the hypergeometric function [27, eq. (7.5)]. $G_{p,q}^{m,n}(.)$ represent Meijer's G-functions [29, eq. (9.3)]. $H_{p,q:u,v:e,f}^{m,n:s,t:i,j}(.)$ represents the extended generalized bivariate Fox-function [30, eq. (2.56)].

II. System Model and Basic Definitions

Fig. 1 depicts the considered network, which consists of a source S, a destination D and an eavesdropper E, all equipped with single antenna. Due to the presence of obstacles, it is postulated that the direct link between S and destination D as well as between the S and E, are obstructed. In this configuration, a system is implemented with an RIS designed as a reflect-array comprising N reconfigurable reflecting elements. Being capable of dynamically controlling the phase shift of its reflecting elements, RIS is expected to improve the communication efficiency. The signals received with the aid of RIS at D and E can be, respectively, expressed as

$$Y_D = \left[\sum_{n=1}^{N} h_{S,n} h_{D,n} e^{-j\phi_n}\right] X + Z_D \tag{1}$$

and

$$Y_E = \left[\sum_{n=1}^{N} h_{S,n} h_{E,n} e^{-j\phi_n}\right] X + Z_E \tag{2}$$

where X denotes the transmit signal by S with power P_s. Additionally, Z_D and Z_E represent the additive white Gaussian noise (AWGN) with zero mean and variances σ_D^2 and σ_E^2 at D and E, respectively. The channel coefficients from S to the nth element of the RIS are represented by $h_{S,n}$, $n \in \{1, 2, \ldots, N\}$, while the channel coefficients from the RIS to nodes D and E are denoted by $h_{i,n}$, where $i \in \{D, E\}$. The

reconfigurable phase induced by the nth reflector of the RIS is represented by ϕ_n, which can be adjusted to maximize the SNR of the received signals via phase matching. We define $h_{S,n}$ and $h_{i,n}$ as $\sqrt{g_{S,n}d_{SR}^{-\alpha}e^{-j\theta_n}}$ and $\sqrt{g_{i,n}d_{Ri}^{-\alpha}e^{-j\psi_{i,n}}}$ for $i \in \{D, E\}$, respectively. d_{SR}, d_{RD}, and d_{RE} denote the distance between S and the RIS, RIS and D, and RIS and E, respectively. $g_{S,n}$, $g_{D,n}$, and $g_{E,n}$ are the amplitudes of the corresponding channel gains, while α denotes the path-loss exponent. $e^{-j\theta_n}$ and $e^{-j\psi_{i,n}}$ represent the phase of the links between S and R and between R and i, respectively, where $i \in \{D, E\}$. Furthermore, similar to [10], [11], [12], and [13], to maximize the instantaneous SNR at D, the optimal ϕ_n admits the form $\phi_n^* = \theta_n + \psi_{D,n}$. Furthermore, we contemplate the most unfavorable circumstance for the secure wireless system incorporating RIS, where E possesses an exceedingly potent detection ability. Consequently, all the signals that have been reflected are assumed to be co-phased. Thus, we have $\psi_{E,n} = \phi_n^* - \theta_n$, indicating that the instantaneous SNR at E is also maximized with the optimal ϕ_n, namely, ϕ_n^*.

Now, based on the definitions provided, the instantaneous SNRs at nodes D and E can be expressed as follows:

$$\gamma_D = \frac{P_s|\sum_{n=1}^{N} g_{S,n}g_{D,n}|}{\sigma_D^2 d_{SR}^{\alpha} d_{RD}^{\alpha}} \tag{3}$$

and

$$\gamma_E = \frac{P_s|\sum_{n=1}^{N} g_{S,n}g_{E,n}|}{\sigma_E^2 d_{SR}^{\alpha} d_{RE}^{\alpha}}. \tag{4}$$

Additionally, the instantaneous capacities of the system for the instantaneous SNRs γ_D and γ_E can be expressed as $C_D = \log_2(1 + \gamma_D)$ and $C_E = \log_2(1 + \gamma_E)$, respectively.

In our analysis, we make the foundational assumption that the fading channel coefficients conform to the Fisher-Snedecor $\mathcal{F}$ distribution, characterized by fading parameters of (m_{s_k}, m_k) [3]. This statistical model plays a crucial role in capturing the stochastic nature of wireless communication channels, providing a framework to understand the variability and unpredictability of the channel coefficients. Specifically, m_{s_k} represents the shadowing effect on the root-mean-square signal power, while m_k denotes the severity parameter of the fading. Under the assumption that all fading channel coefficients are characterized by independent Fisher-Snedecor F distribution, the PDF and CDF of the instantaneous SNRs at D and E are respectively determined as follows [16]:

$$f_{\gamma_i}(\gamma_i) = \frac{(\frac{\gamma_i}{\bar{\gamma}_i})^{(\frac{a_i}{2})}}{2\Gamma(a_i+1)\sqrt{\gamma_i\bar{\gamma}_i}b_i^{a_i+1}} e^{-\frac{1}{b_i}\sqrt{\frac{\gamma_i}{\bar{\gamma}_i}}} \tag{5}$$

and

$$F_{\gamma_i}(\gamma_i) = \frac{\gamma(a_i+1, \frac{1}{b_i}\sqrt{\frac{\gamma_i}{\bar{\gamma}_i}})}{\Gamma(a_i+1)} \tag{6}$$

where $i \in \{D, E\}$, $\bar{\gamma}_i$ denotes the average SNR at i, $a_i = (NB_i^2)/(B_i^2 - A_iC_i) - 1$, $b_i = B_i/(C_iD_i)[1 - (A_iC_i)/(B_i^2)]$, $A_i = B(m_R + 1, m_{s_R} - 1)B(m_i + 1, m_{s_i} - 1)$, $B_i = B(m_R + (1/2), m_{s_R} - (1/2))B(m_i + (1/2), m_{s_i} - (1/2))$, $C_i = B(m_R, m_{s_R})B(m_i, m_{s_i})$, and $D_i = [(m_Rm_i)/(\Omega_R\Omega_i(1 - m_{s_R})(1 - m_{s_i}))]^{(1/2)}$ where Ω_k for $k \in \{R, D, E\}$ is the mean power.

III. Secrecy Performance Analysis

In this section, analytical expressions are derived for the ASC and SOP of the system over correlated Fisher-Snedecor $\mathcal{F}$ fading channels. The results provide a theoretical framework for understanding the system's performance characteristics, which can be used for system design and optimization. The analytical derivations are based on the statistical characterization of the instantaneous SNRs at the D and E nodes.

A. ASC Analysis

The ASC is a key performance metric in secure communication systems. It represents the average rate at which secure information can be transmitted over the communication channel, while keeping the information hidden from unauthorized users. The ASC for the considered system model can be defined as follows [4]:

$$\bar{C}_s = \int_0^{\infty}\int_{\gamma_E}^{\infty} C_s(\gamma_D, \gamma_E) f(\gamma_D, \gamma_E) d\gamma_D d\gamma_E \tag{7}$$

where $f(\gamma_D, \gamma_E)$ is the joint PDF of γ_D and γ_E and C_s is the instantaneous secrecy capacity, which is defined as:

$$C_s(\gamma_D, \gamma_E) = [C_D - C_E]^+. \tag{8}$$

We assume that the fading channels under consideration exhibit correlation. Therefore, it is imperative to establish a suitable mathematical model for obtaining the joint PDF, $f(\gamma_D, \gamma_E)$. In order to accomplish this, we provide a concise overview of the copula theory [18], [19], which is a powerful mathematical tool used to model multivariate distributions.

The copula function is a crucial mathematical tool in wireless communication systems, providing a versatile framework for modeling complex dependencies among channel components [19]. Unlike traditional linear correlation measures, copulas adaptively capture intricate patterns, especially in wireless channels with nonlinear and asymmetrical correlations [22]. Their flexibility aligns seamlessly with the dynamic nature of wireless communication environments. Copulas also play a vital role in separating marginal distributions, allowing a focused exploration of the underlying correlation structure [23]. As wireless networks evolve, copulas serve as indispensable tools for understanding and optimizing system performance in the face of connectivity and reliability challenges.

Incorporating copulas into our analysis allows us to delve deeper into the underlying dynamics of channel correlation. By leveraging their flexibility, ability to capture tail dependencies, and capacity to model various dependency structures, we can unveil insights that might otherwise remain obscured by traditional approaches. Ultimately, copulas enable a more comprehensive understanding of the complex interplay between channel components, contributing to a richer analysis of the correlation effects on wireless communication systems.

Definition 1 (Two-Dimensional Copula): Consider a vector $V = (v_1, v_2)$ comprising two RVs and their corresponding marginal CDFs, denoted as $F(v_j) = \Pr(V_j \le v_j)$ for $j = 1, 2$. In this context, the relevant bivariate CDF can be expressed as follows:

$$F(v_1, v_2) = \Pr(V_1 \le v_1, V_2 \le v_2). \tag{9}$$

Then, consider the copula function $C(u_1, u_2)$ of the vector $V = (v_1, v_2)$, which is defined on the unit hypercube $[0, 1]^2$. The RVs $U_j = F(v_j)$ for $j = 1, 2$ are uniformly distributed over the interval [0, 1]. The expression for the copula function is then given by [18]

$$C(u_1, u_2) = \Pr(U_1 \leq u_1, U_2 \leq u_2). \tag{10}$$

Theorem 1 (Sklar's Theorem): Consider a joint CDF, denoted as $F(v_1, v_2)$, for two RVs with marginal CDFs $F(v_j)$ for $j = 1, 2$. For any v_j belonging to the extended real line domain $\mathbb{R}$, there exists a copula function C that can be used to express the relationship between the joint CDF and the copula function in the following manner [18]:

$$F(v_1, v_2) = C(F(v_1), F(v_2)). \tag{11}$$

The joint PDF $f(v_1, v_2)$ can be obtained by applying the chain rule to (11), resulting in the following expression [18]

$$f(v_1, v_2) = f(v_1) f(v_2) c(F(v_1), F(v_2)) \tag{12}$$

where $c(F(v_1), F(v_2)) = ([\partial^2 C(F(v_1), F(v_2))]/[\partial F(v_1) \partial F(v_2)])$ is the copula density function and $f(v_j)$ for $j = 1, 2$ are the marginal PDFs, respectively.

Despite the existence of numerous copula types, we have chosen to utilize the FGM copula function in our analysis of the performance metrics of the proposed system model. This decision is based on FGM copula's ability to quickly process statistical data, as well as its use of simple closed form expressions and adherence to general mathematical constructions, as described in previous literature [31].

Definition 2 (FGM Copula): The FGM copula, which is characterized by a dependence parameter $\theta \in [-1, 1]$, is given by

$$C_F(u_1, u_2) = u_1 u_2 (1 + \theta(1 - u_1)(1 - u_2)) \tag{13}$$

where $\theta \in [-1, 0]$ and $\theta \in [0, 1]$ denote the negative and positive dependence structures, respectively. In addition, the value of $\theta = 0$ signifies an independence structure between the relevant variables.

By employing partial derivatives on (13), incorporating the obtained results into (12), and subsequently analyzing the marginal distribution of SNRs, we determine the joint PDF of γ_D and γ_E as follows [18], [23]:

$$f(\gamma_D, \gamma_E) = f_1 + \theta(f_1 - 2f_2 - 2f_3 + 4f_4), \tag{14}$$

where $f_1 = f_{\gamma_D}(\gamma_D) f_{\gamma_E}(\gamma_E)$, $f_2 = f_{\gamma_D}(\gamma_D) f_{\gamma_E}(\gamma_E) F_{\gamma_E}(\gamma_E)$, $f_3 = f_{\gamma_D}(\gamma_D) f_{\gamma_E}(\gamma_E) F_{\gamma_D}(\gamma_D)$, and $f_4 = f_{\gamma_D}(\gamma_D) f_{\gamma_E}(\gamma_E) F_{\gamma_D}(\gamma_D) F_{\gamma_E}(\gamma_E)$.

Theorem 2: The expression for the ASC in the analyzed secure communication system with RIS assistance, operating in correlated Fisher-Snedecor $\mathcal{F}$ fading channels, is given by (15), shown at the bottom of the page, where $h = (\Gamma(a_D + 1)\Gamma(a_E + 1)\ln(2))^{-1}$, $\tau = \frac{2^{a_E}}{\sqrt{\pi}\Gamma(a_E+1)\ln(2)}$, $M_1 = h(2(1 + [b_D/b_E]\sqrt{[\bar{\gamma}_D/\bar{\gamma}_E]})^{(a_D+1)}(1 + [b_E/b_D]\sqrt{[\bar{\gamma}_E/\bar{\gamma}_D]})^{(a_E+1)})^{-1}$, $m_1 = ((1 + [b_E/b_D]\sqrt{[\bar{\gamma}_E/\bar{\gamma}_D]})^k \Gamma(a_E + 2 + k))^{-1}$, $m_2 = ((1 + [b_D/b_E]\sqrt{[\bar{\gamma}_D/\bar{\gamma}_E]})^k \Gamma(a_D + 2 + k))^{-1}$, $M_3' = [2/3](1 + ([\Gamma(a_D + 1)/\Gamma(a_E + 1)])^2)(2(1 + [2b_D/b_E]\sqrt{[\bar{\gamma}_D/\bar{\gamma}_E]})^{(a_D+1)}(1 + [2b_E/b_D]\sqrt{[\bar{\gamma}_E/\bar{\gamma}_D]})^{2(a_E+1)}(\Gamma(a_D + 1))^2 \ln(2))^{-1}$, $m_3 = ([_2F_1(1, -(k + a_E + 1); a_E + 2; -1)]/ [\Gamma(a_E + 2)\Gamma(k + a_E + 2)] - [_2F_1(1, -a_E; k + a_E + 3; -1)]/ [\Gamma(a_E + 1)\Gamma(k + a_E + 3)])(2 + (b_E/b_D)\sqrt{[\bar{\gamma}_E/\bar{\gamma}_D]})^{-k}$, $m_3' = ([_2F_1(1, -(k + a_D + 1); a_D + 2; -1)]/[\Gamma(a_D + 2)\Gamma(k + a_D + 2)] - [_2F_1(1, -a_D; k + a_D + 3; -1)]/[\Gamma(a_D + 1)\Gamma(k + a_D + 3)])(2 + [b_D/b_E]\sqrt{[\bar{\gamma}_D/\bar{\gamma}_E]})^{-k}$, $u_{11} = u_{12} = u_{13} = ([1/b_D\sqrt{\bar{\gamma}_D}] + [1/b_E\sqrt{\bar{\gamma}_E}])^{-2}$, $\nu_1 = (-a_D, 2; 1)$, $\acute{\nu_1} = (-a_E, 2; 1)$, $\nu_2 = \acute{\nu_2} = (1, 1; 1), (1, 1; 1)$, $\nu_3 = \acute{\nu_3} = (1, 1; 1)$, $\omega_2 = \acute{\omega_2} = (1, 1), (0, 1; 1)$, $\omega_3 = (a_E + 1, 1), (0, 1; 1)$, $\acute{\omega_3} = (a_D + 1, 1), (0, 1; 1)$, $\nu_{11} = \nu_{12} = (-(1 + a_D + a_E + k), 2; 1)$, $\nu_{13} = (-(1 + a_D + 2a_E + k), 2; 1)$, $\nu_{23} = \nu_{23}' = \nu_2$, $\nu_{21} = \nu_{22} = \nu_{32} = \nu_{31} = \nu_{33} = \nu_3$, $\omega_{21} = \omega_{22} = \omega_{23} = \omega_{23}' = (1, 1)$, $\omega_{31} = \omega_3$, $\omega_{32} = \omega_{33} = \omega_3'$, $\nu_{33} = \nu_{33}' = (1, 1; 1)$, $\nu_{13}' = (-(1 + a_E + 2a_D + k), 2; 1)$, and $\omega_{33}' = (a_E + 1, 1), (0, 1; 1)$.

Proof: The detailed proof is given in Appendix A. ■

Remark 1: It is important to highlight that for the particular case of $\theta = 0$, the derived results in Theorem 2 reduce to the case of independent fading.

B. SOP Analysis

The SOP is an information-theoretical metric used to assess the performance of PLS. This metric is defined as the probability that the instantaneous secrecy capacity C_s falls below a specified target secrecy rate R_s, where R_s is a positive value, as follows [4]:

$$P_{sop} = \Pr(C_s \leq R_s). \tag{16}$$

Theorem 3: The expression for the SOP in the analyzed secure communication system with RIS assistance, operating

$$\begin{aligned}
\bar{C}_s = h(1+\theta)\Bigg(& H_{1,0:2,2:1,2}^{0,1:1,2:1,1}\left(b_D^2\bar{\gamma}_D, \frac{b_D}{b_E}\sqrt{\frac{\bar{\gamma}_D}{\bar{\gamma}_E}} \,|\, {}_{-}^{\nu_1} \,|\, {}_{\omega_2}^{\nu_2} \,|\, {}_{\omega_3}^{\nu_3}\right) + H_{1,0:2,2:1,2}^{0,1:1,2:1,1}\left(b_E^2\bar{\gamma}_E, \frac{b_E}{b_D}\sqrt{\frac{\bar{\gamma}_E}{\bar{\gamma}_D}} \,|\, {}_{-}^{\acute{\nu}_1} \,|\, {}_{\omega_2'}^{\nu_2'} \,|\, {}_{\omega_3'}^{\nu_3'}\right)\Bigg) \\
& - \tau G_{4,2}^{1,4}\left(4\left(b_E\sqrt{\bar{\gamma}_E}\right)^2 \,|\, {}_{1,0}^{-\frac{a_E}{2}, \frac{1-a_E}{2}, 1, 1}\right) - 6\theta\left(M_1 \sum_{k=0}^{\infty} m_1 H_{1,0:1,2:1,2}^{0,1:1,1:1,1}\left(u_{11}, \left(1 + \frac{b_E}{b_D}\sqrt{\frac{\bar{\gamma}_E}{\bar{\gamma}_D}}\right)^{-1} \,|\, {}_{-}^{\nu_{11}} \,|\, {}_{\omega_{21}}^{\nu_{21}} \,|\, {}_{\omega_{31}}^{\nu_{31}}\right) - M_1\right. \\
& \sum_{k=0}^{\infty} m_2 H_{1,0:1,2:1,2}^{0,1:1,1:1,1}\left(u_{12}, \left(1 + \frac{b_D}{b_E}\sqrt{\frac{\bar{\gamma}_D}{\bar{\gamma}_E}}\right)^{-1} \,|\, {}_{-}^{\nu_{12}} \,|\, {}_{\omega_{22}}^{\nu_{22}} \,|\, {}_{\omega_{32}}^{\nu_{32}}\right) - M_3' \sum_{k=0}^{\infty} m_3 H_{1,0:2,2:1,2}^{0,1:1,2:1,1}\left(u_{13}, \left(1 + \frac{2b_D}{b_E}\sqrt{\frac{\bar{\gamma}_D}{\bar{\gamma}_E}}\right)^{-1} \,|\, {}_{-}^{\nu_{13}} \,|\, {}_{\omega_{23}}^{\nu_{23}} \,|\, {}_{\omega_{33}}^{\nu_{33}}\right) \\
& \left. + M_3' \sum_{k=0}^{\infty} m_3' H_{1,0:2,2:1,2}^{0,1:1,2:1,1}\left(u_{13}, \left(1 + \frac{2b_D}{b_E}\sqrt{\frac{\bar{\gamma}_D}{\bar{\gamma}_E}}\right)^{-1} \,|\, {}_{-}^{\nu_{13}'} \,|\, {}_{\omega_{23}'}^{\nu_{23}'} \,|\, {}_{\omega_{33}'}^{\nu_{33}'}\right)\right)
\end{aligned} \tag{15}$$

in correlated Fisher-Snedecor $\mathcal{F}$ fading channels is given by

$$P_{\text{sop}} = \varrho\Bigg[\theta_1 H^{0,1:1,1:1,1}_{1,0:1,1:2,2}\Big(u_3, \eta_3 \,|\, {}^{\nu_1''}_{-} \,|\, {}^{\nu_2''}_{\omega_2''} \,|\, {}^{\nu_3''}_{\omega_3''}\Big) + \theta_2 \sum_{k=0}^{\infty}\sum_{k'=0}^{\infty} \varepsilon\Big(H^{0,1:0,1:2,1}_{1,0:1,1:1,4}\Big(u_3, \eta_3 \,|\, {}^{\nu_{11}''}_{-} \,|\, {}^{\nu_{21}''}_{\omega_{21}''} \,|\, {}^{\nu_{31}''}_{\omega_{32}''}\Big) - \frac{2}{\Gamma(a_E+1)} H^{0,1:1,1:2,1}_{1,0:1,2:1,4}\Big(u_3, \eta_3 \,|\, {}^{\nu_{11}''}_{-} \,|\, {}^{\nu_{21}''}_{\omega_{21}''} \,|\, {}^{\nu_{31}''}_{\omega_{32}''}\Big)\Big)\Bigg] \quad (17)$$

where $\varrho = (1 - 1/(2^{R_s}))(1/(b_E\sqrt{\bar{\gamma}_E}))^2 1/(\Gamma(a_D+1)\Gamma(a_E+1))$, $\theta_1 = (1 + \theta - [2\theta/\Gamma(a_E+1)])$, $\theta_2 = \theta([\Gamma(a_D+1)/\sqrt{\pi}])([1-2^{R_s}]/[(b_D\sqrt{\bar{\gamma}_D})^2])^{(a_D+1)}$, $\varepsilon = ((b_D\sqrt{[\bar{\gamma}_D/2^{R_s}-1]})^{(k+k')}\Gamma(a_D+2+k)\Gamma(a_D+2+k'))^{-1}$, $u_3 = b_E^2\bar{\gamma}_E(1+\frac{1}{2^{R_s}-1})$, $\eta_3 = b_D\sqrt{\frac{\bar{\gamma}_D}{2^{R_s}-1}}$, $\nu_1'' = (2, \frac{1}{2}; 1)$, $\nu_2'' = (2-a_E, 2)$, $\nu_3'' = (-a_D, 1; 1), (1,1)$, $\omega_2'' = (1,1)$, $\omega_3'' = (0,1), (1, \frac{1}{2}; 1)$, $\nu_{11}'' = (a_D + 3 + [k+k'/2], 1; 1)$, $\nu_{21}'' = (2-a_E, 1; 1)$, $\nu_{31}'' = (-(a_D + 1 + [k+k'/2]), 1; 1)$, $\omega_{21}'' = (1,1), (1,1; 1)$, and $\omega_{32}'' = (0,1), (1/2, 1), (0, 1; 1), (1/2, 1; 1)$.

Proof: The detailed proof is given in Appendix B. ∎

Remark 2: It is important to highlight that for the particular case of $\theta = 0$, the SOP results in Theorem 3 reduce to the case of independent fading.

The mathematical equations obtained for the performance measures seem complex at a first glance. This complexity primarily stems from the intricate nature of channel modeling and the interactions among different factors. To tackle this challenge and offer a clearer view of the possible results when altering system parameters, we delve into studying the asymptotic behavior of the derived secrecy metrics in the following section. More specifically, we will strive to clarify the intuitive meanings of key parameters and how they influence the system's performance. Our goal is to provide insights into the connections between these parameters and the resulting metrics, aiming to enhance the overall understanding of the implications that come with adjusting these parameters.

IV. Asymptotic Analysis of Secrecy Metrics

In this section, we examine the asymptotic behavior of both ASC and SOP to illustrate the impact of channel parameters and gain a deeper understanding of how secrecy metrics behave across various dimensions. In this context, we exploit the expansions associated with both univariate and bivariate Fox's H-functions. These expansions are derived by evaluating the residue of the corresponding integrands at the nearest poles to the contour. Specifically, we consider the minimum pole on the right for large Fox's H-function arguments and the maximum pole on the left for small arguments, as elaborated in [32].

A. Asymptotic ASC Analysis

With respect to the analytical expression obtained for ASC as presented in (15), within the high SNR regime, namely when $\bar{\gamma}_D \to \infty$, the asymptotic ASC can be established according to the following theorem.

Theorem 4: In the high-SNR regime, where $\bar{\gamma}_D \to \infty$, the asymptotic expression for the corresponding ASC under the correlated Fisher-Snedecor $\mathcal{F}$ fading channels is given by

$$\bar{C}_s^{\text{asy}} = \left[\tau_1\left(\left(\frac{1}{b_D\sqrt{\bar{\gamma}_D}}\right)^{(a_E+a_D+2)} + \left(\frac{1}{b_E\sqrt{\bar{\gamma}_E}}\right)^{(a_E+a_D+2)}\right) + 2\tau_2\right](1+\theta) - \tau G^{1,4}_{4,2}\left(4\left(b_E\sqrt{\bar{\gamma}_E}\right)^2 \,|\, {}^{-\frac{a_E}{2}, \frac{1-a_E}{2}, 1, 1}_{1,0}\right) - 6\theta\left(\frac{m_{11}+m_{21}}{2\ln(2)\left(b_D\sqrt{\bar{\gamma}_D}+b_E\sqrt{\bar{\gamma}_E}\right)^{(a_D+a_E+2)}} - \frac{2}{3}(m_{31}+m_{32})\right) \quad (18)$$

where

$$\tau_1 = \frac{\frac{\Gamma(\frac{a_D+a_E+4}{2})\Gamma^2(-\frac{a_D+a_E+2}{2})}{\Gamma(-\frac{a_D+a_E}{2})}}{\ln(2)(b_D\sqrt{\bar{\gamma}_D})^{(a_D+1)}(b_E\sqrt{\bar{\gamma}_E})^{(a_E+1)}\Gamma(a_D+1)\Gamma(a_E+2)},$$

$$\tau_2 = \frac{\Gamma(a_D+a_E+2)}{\ln(2)(b_D\sqrt{\bar{\gamma}_D})^{(a_D+1)}(b_E\sqrt{\bar{\gamma}_E})^{(a_E+1)}\Gamma(a_D+1)\Gamma(a_E+2)},$$

$$\tau = \frac{2^{a_E}}{\sqrt{\pi}\Gamma(a_E+1)\ln(2)},$$

$$m_{11} = \left(\left(1+\frac{b_E}{b_D}\sqrt{\frac{\bar{\gamma}_E}{\bar{\gamma}_D}}\right)^{(a_E+1)}\Gamma(a_D+1)\Gamma(a_E+2)\right)^{-1}\left(\Gamma(a_D+2a_E+k+3) + \left(\frac{1}{b_D\sqrt{\bar{\gamma}_D}}+\frac{1}{b_E\sqrt{\bar{\gamma}_E}}\right)^{(a_D+2a_E+k+3)} \times \frac{\Gamma\left(\frac{a_D+2a_E+k+5}{2}\right)\Gamma^2\left(-\frac{a_D+2a_E+k+3}{2}\right)}{\Gamma\left(-\frac{a_D+2a_E+k+1}{2}\right)}\right), m_{21}$$

$$= \left(\left(1+\frac{b_D}{b_E}\sqrt{\frac{\bar{\gamma}_D}{\bar{\gamma}_E}}\right)^{(a_D+1)}\Gamma(a_E+1)\Gamma(a_D+2)\right)^{-1}\left(\Gamma(2a_D+a_E+k+3) + \left(\frac{1}{b_E\sqrt{\bar{\gamma}_E}}+\frac{1}{b_D\sqrt{\bar{\gamma}_D}}\right)^{(2a_D+a_E+k+3)} \times \frac{\Gamma\left(\frac{2a_D+a_E+k+5}{2}\right)\Gamma^2\left(-\frac{2a_D+a_E+k+3}{2}\right)}{\Gamma\left(-\frac{2a_D+a_E+k+1}{2}\right)}\right), m_{31}$$

$$= \frac{\left(\frac{1}{b_D\sqrt{\bar{\gamma}_D}}+\frac{2}{b_E\sqrt{\bar{\gamma}_E}}\right)^{-2(a_D+a_E+2)}}{\ln(2)\left(b_E\sqrt{\bar{\gamma}_E}\right)^{2(a_E+1)}\Gamma(a_D+1)\Gamma(a_E+2)} \times \Bigg(\left(\frac{1}{b_D\sqrt{\bar{\gamma}_D}}+\frac{2}{b_E\sqrt{\bar{\gamma}_E}}\right)^{(2a_D+2a_E+3)}\sum_{k=0}^{\infty} m_3\left(b_E\sqrt{\bar{\gamma}_E}\right)^{-k} \frac{\Gamma\left(\frac{2a_D+2a_E+k+4}{2}\right)\Gamma^2\left(-\frac{2a_D+2a_E+k+3}{2}\right)}{\Gamma\left(-\frac{2a_D+2a_E+k+1}{2}\right)} + \left(\frac{1}{1+\frac{2b_D}{b_E}\sqrt{\frac{\bar{\gamma}_D}{\bar{\gamma}_E}}}\right)^{a_D}\sum_{k=0}^{\infty} m_3\left(\frac{b_D}{b_E}\sqrt{\frac{\bar{\gamma}_D}{\bar{\gamma}_E}}\right)^{-k} \Gamma(2a_D+2a_E+k+3)\Bigg),$$

and

$$m_{32} = \frac{\left(\frac{2}{b_D\sqrt{\bar{\gamma}_D}}+\frac{1}{b_E\sqrt{\bar{\gamma}_E}}\right)^{-2(a_D+a_E+2)}}{\ln(2)\left(b_D\sqrt{\bar{\gamma}_D}\right)^{2(a_D+1)}\Gamma(a_E+1)\Gamma(a_D+2)}$$

$$\left(\left(\frac{2}{b_D\sqrt{\bar{\gamma}_D}}+\frac{1}{b_E\sqrt{\bar{\gamma}_E}}\right)^{(2a_D+2a_E+3)}\right.$$
$$\sum_{k=0}^{\infty} m_3'\left(b_D\sqrt{\bar{\gamma}_D}\right)^{-k}\frac{\Gamma\left(\frac{2a_D+2a_E+k+4}{2}\right)\Gamma^2\left(-\frac{2a_D+2a_E+k+3}{2}\right)}{\Gamma\left(-\frac{2a_D+2a_E+k+1}{2}\right)}$$
$$\left.+\left(\frac{1}{1+\frac{2b_E}{b_D}\sqrt{\frac{\bar{\gamma}_E}{\bar{\gamma}_D}}}\right)^{a_E}\sum_{k=0}^{\infty} m_3'\left(\frac{b_E}{b_D}\sqrt{\frac{\bar{\gamma}_E}{\bar{\gamma}_D}}\right)^{-k}\Gamma(2a_D+2a_E+k+3)\right).$$

Proof: The detailed proof is given in Appendix C. ■

B. Asymptotic SOP Analysis

By applying the same analytical approach employed in the derivation of the asymptotic ASC, we deduce the asymptotic expression for the SOP within the high SNR regime, as presented in the following theorem.

Theorem 5: In the high-SNR regime, where $\bar{\gamma}_D \to \infty$, the asymptotic expression for the corresponding SOP under the correlated Fisher-Snedecor $\mathcal{F}$ fading channels is given by

$$P_{\text{sop}}^{\text{asy}} = \frac{\Gamma(a_D+a_E+2)}{\Gamma(a_D+2)\Gamma(a_E+1)}\left(\frac{b_E}{b_D}\sqrt{\frac{2^{R_s}\bar{\gamma}_E}{\bar{\gamma}_D}}\right)^{(a_D+1)}$$
$$\left(1+\theta\left(1-\frac{2}{\Gamma(a_E+1)}\right)\right)-\frac{16\pi\sqrt{\pi}}{\Gamma(a_E+1)}\psi\theta \quad (19)$$

where

$$\psi = \frac{\left(2^{R_s}\right)^{(a_D+1)}\left(b_E^2\bar{\gamma}_E\right)^{\left(a_D+\frac{3}{2}\right)}}{\left(b_D^2\bar{\gamma}_D\right)^{\left(a_D+\frac{3}{4}\right)}}\left(\frac{1}{\sqrt{2^{R_s}-1}}\left(\frac{1}{1-2^{R_s}}-1\right)\right)^{\frac{1}{2}}$$
$$\sum_{k=0}^{\infty}\sum_{k'=0}^{\infty}\left(\left(\frac{1}{1-2^{R_s}}-1\right)b_E^2\bar{\gamma}_E\right)^{\left(\frac{k+k'}{2}\right)}$$
$$\times\left(1-2\Gamma\left(-a_D+\frac{3}{2}+\frac{k+k'}{2}\right)\right).$$

Proof: The detailed proof is given in Appendix D. ■

It can be noted that the expressions for the ASC and SOP, which are initially represented in terms of the bivariate Fox's H-function, can be effectively transformed into a simplified mathematical representation at high SNR regime. This simplification is achieved through the utilization of the residue approach. We can also observe that these theorems provide an approximation of the ASC and SOP when SNR is extremely high, offering valuable insights into the system's performance under ideal conditions.

V. Numerical Results

In this section, we conduct a thorough evaluation of the theoretical expressions that were derived earlier. To ensure their reliability, we subject them to rigorous scrutiny by means of Monte-Carlo simulations, with this validation process applied consistently across all instances. We incorporate fading parameters (m_{s_k}, m_k) into our study based on the findings presented in reference [4], [32], [33], [34], [35]. Besides, it is important to note that the implementation of the extended generalized bivariate Fox's H-function is currently not available in popular mathematical software packages. Nonetheless, it is noteworthy that this implementation remains computationally feasible and programmable, as presented in [36]. Furthermore, the fundamental simulation of copula-based dependence between RVs can be readily executed using mathematical software packages like MATLAB. For more advanced functionalities in this context, researchers can leverage recently developed packages as referenced in [37]. It is assumed that the source power is $P_s = 20$ W, $d_{SR} = d_{RD} = d_{RE} = 10$ m, $\bar{\gamma}_E = 5$ dB, $R_s = 1$, $\alpha = 2.7$, $\sigma_D = \sigma_E = 1$, and $(m_{s_k}, m_k) = (3, 2)$ for $k \in \{R, D, E\}$.

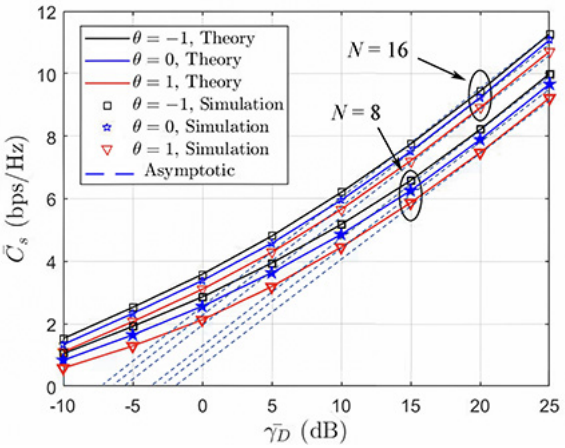

Fig. 2. ASC versus $\bar{\gamma}_D$ at specific values of N and dependence parameter θ.

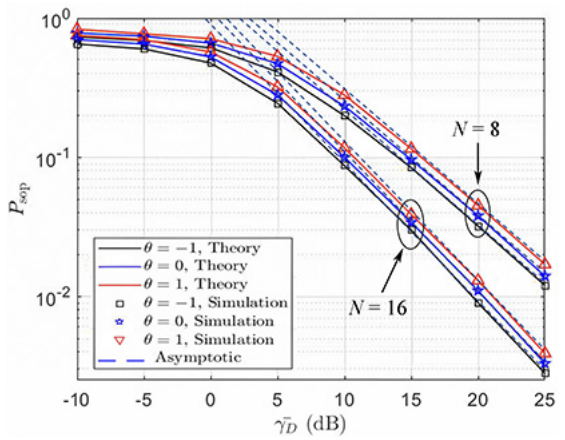

Fig. 3. SOP versus $\bar{\gamma}_D$ at specific values of N and dependence parameter θ.

Fig. 2 illustrates the performance of ASC under correlated Fisher-Snedecor $\mathcal{F}$ fading channels based on the variation of $\bar{\gamma}_D$ for selected values of N and dependence parameter θ. It can be observed that in the presence of positive dependence, the performance of ASC deteriorates compared to the independent fading scenario. This is due to the fact that as the correlation between channels increases, their behavior becomes more alike, resulting in a reduced likelihood of the transmitter being able to achieve a high-secrecy rate. On the other hand, when negative dependence is present, the correlated fading performs better than the uncorrelated fading scenario for ASC. Fig. 3 illustrates the performance of SOP in terms of $\bar{\gamma}_D$ under correlated Fisher-Snedecor $\mathcal{F}$ fading channels for different values of N and dependence parameter θ. It can be observed that under negative dependence structure, correlated fading yields a smaller SOP compared to positive correlation and independent cases. From

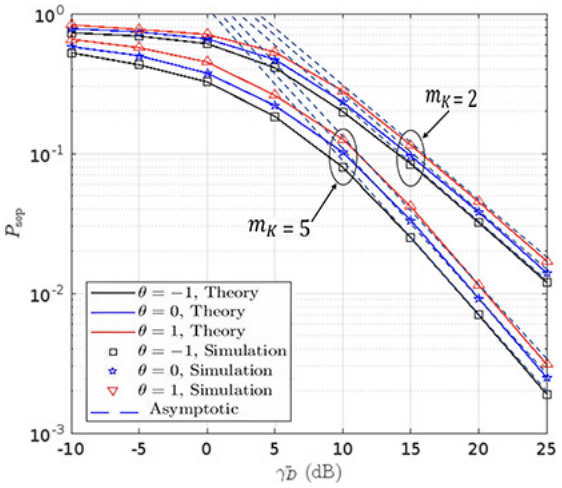

Fig. 4. SOP versus $\bar{\gamma}_D$ at specific values of m_k and θ, when $N = 8$.

Figs. 2 and 3, we observe that increasing the number of RIS elements N, leads to superior ASC and SOP performance, respectively. Moreover, it can be seen in all these plots that the simulation results match very well with the theoretical ones, verifying the accuracy of the analysis. Fig. 4 further plots the SOP performance versus $\bar{\gamma}_D$, for different fading parameter values m_k and dependence parameter θ when $N = 8$. It can be observed that as the values of m_k increases, the system's SOP performance improves. This aligns with the fundamental tenet of how PLS strategically exploits the stochastic properties of wireless channels, particularly fading, to fortify the confidentiality of communication systems. Additionally, it is worth highlighting that the asymptotic results align closely with the other findings, particularly in high-SNR regions. This further corroborates the robustness and applicability of the analysis.

VI. Conclusion

In this article, we studied the PLS performance within a network architecture incorporating a relay system based on RIS, strategically positioned on a building, in the presence of an eavesdropper. Through the derivation of closed-form equations for the PDF and CDF of the SNRs at both the destination and eavesdropper, analytical expressions for the ASC and SOP were determined for Fisher-Snedecor $\mathcal{F}$ fading channels under correlated fading coefficients. We also analyzed the asymptotic behavior of the obtained secrecy metrics. Furthermore, numerical simulations were performed to validate the theoretical results and to show the impact of various channel parameters on the ASC and SOP performances. The results of this study demonstrated that augmenting the number of reflecting elements in RIS can enhance the performance of wireless communication schemes. These results can have significant implications for the design and optimization of future wireless communication systems.

Looking forward, exploring the impact of multiple eavesdroppers presents an intriguing avenue for future research. Understanding how such scenarios alter the dynamics of PLS in RIS-aided networks could yield valuable insights for enhancing security in wireless communications systems.

Appendix A
Proof of Theorem 2

By inserting (8) into (7), and applying the joint PDF $f(\gamma_D, \gamma_E)$ expressed in (14), $\bar{C}_s$ can be expressed as

$$\bar{C}_s = J_1 - J_2 \tag{20}$$

where

$$\begin{aligned} J_1 &= \int_0^{\infty}\int_0^{\gamma_D} \log_2(1+\gamma_D) f(\gamma_D, \gamma_E) d\gamma_E d\gamma_D \\ &= k_1 + \theta(k_1 - 2k_2 - 2k_3 + 4k_4) \end{aligned} \tag{21}$$

and

$$\begin{aligned} J_2 &= \int_0^{\infty}\int_{\gamma_E}^{\infty} \log_2(1+\gamma_E) f(\gamma_D, \gamma_E) d\gamma_D d\gamma_E \\ &= A_1 + \theta(A_1 - 2A_2 - 2A_3 + 4A_4). \end{aligned} \tag{22}$$

By substituting the marginal distribution from (5) and (6) into (7), and re-expressing the logarithm function and the incomplete Gamma function in terms of the Meijer's G-function [24], k_1 can be determined as

$$\begin{aligned} k_1 = k_{11} \int_0^{\infty} & \gamma_D^{\frac{a_D-1}{2}} e^{-\frac{1}{b_D}\sqrt{\frac{\gamma_D}{\bar{\gamma}_D}}} \\ & G_{2,2}^{1,2}\left(\gamma_D \middle| \begin{matrix} 1,1 \\ 1,0 \end{matrix}\right) G_{1,2}^{1,1}\left(\frac{1}{b_E}\sqrt{\frac{\gamma_D}{\bar{\gamma}_E}} \middle| \begin{matrix} 1 \\ a_E+1,0 \end{matrix}\right) d\gamma_D \end{aligned} \tag{23}$$

$$\begin{aligned} = \left(\frac{k_{11}}{2\pi j}\right) \int_{l_1} \frac{\Gamma(s)\Gamma(s)\Gamma(1-s)}{\Gamma(1+s)} & \int_0^{\infty} \gamma_D^{\frac{a_D-1+2s}{2}} e^{-\frac{1}{b_D}\sqrt{\frac{\gamma_D}{\bar{\gamma}_D}}} \\ & G_{1,2}^{1,1}\left(\frac{1}{b_E}\sqrt{\frac{\gamma_D}{\bar{\gamma}_E}} \middle| \begin{matrix} 1 \\ a_E+1,0 \end{matrix}\right) d\gamma_D ds \end{aligned} \tag{24}$$

where $k_{11} = (2b_D^{a_D+1}\Gamma(a_D+1)\Gamma(a_E+1)\bar{\gamma}_D^{(a_D+1)/2}\ln(2))^{-1}$ and (23) is obtained by using the definition of the Meijer's function. Using the aid of [38, eq. (2.24.3.1)], we can calculate the inner integral of (24) as $2(b_D\sqrt{\bar{\gamma}_D})^{(a_D+2s+1)} G_{2,2}^{1,2}\left(b_D/b_E\sqrt{\frac{\bar{\gamma}_D}{\bar{\gamma}_E}} \middle| \begin{matrix} -(a_D+2s),1 \\ a_E+1,0 \end{matrix}\right)$. Now, by inserting the derived result for inner integral into (24), we have

$$\begin{aligned} k_1 = 2k_{11}\left(\frac{1}{2\pi j}\right)^2 & (b_D\sqrt{\bar{\gamma}_D})^{(a_D+1)} \\ & \int_{l_1}\int_{l_2} (b_D\sqrt{\bar{\gamma}_D})^{(2s)} \left(\frac{b_D}{b_E}\sqrt{\frac{\bar{\gamma}_D}{\bar{\gamma}_E}}\right)^{\xi} \Gamma(1+a_D+2s+\xi) \\ & \frac{\Gamma(1-s)\Gamma(s)\Gamma(s)\Gamma(a_E+1-\xi)\Gamma(\xi)}{\Gamma(1+s)\Gamma(1+\xi)} d\xi ds. \end{aligned} \tag{25}$$

Consequently, through the recognition of the definition of the bivariate Fox H-function [30], k_1 is derived as:

$$k_1 = hH_{1,0:2,2:1,2}^{0,1:1,2:1,1}\left(b_D^2\bar{\gamma}_D, \frac{b_D}{b_E}\sqrt{\frac{\bar{\gamma}_D}{\bar{\gamma}_E}} \middle| \begin{matrix} \nu_1 \\ - \end{matrix} \middle| \begin{matrix} \nu_2 \\ \omega_2 \end{matrix} \middle| \begin{matrix} \nu_3 \\ \omega_3 \end{matrix}\right) \tag{26}$$

where $h = (\Gamma(a_D+1)\Gamma(a_E+1)\ln(2))^{-1}$, $\nu_1 = (-a_D, 2; 1)$, $\nu_2 = (1, 1; 1), (1, 1; 1)$, $\nu_3 = (1, 1; 1)$, $\omega_2 = (1, 1), (0, 1; 1)$, and $\omega_3 = (a_E+1, 1), (0, 1; 1)$. Afterwards, k_2 can be determined as shown below

$$\begin{aligned} k_2 &= \int_0^{\infty}\int_0^{\gamma_D} \log_2(1+\gamma_D) f_{\gamma_D}(\gamma_D) f_{\gamma_E}(\gamma_E) F_{\gamma_E}(\gamma_E) d\gamma_E d\gamma_D \\ &= \frac{1}{2}\int_0^{\infty} \log_2(1+\gamma_D) f_{\gamma_D}(\gamma_D) \left(F_{\gamma_E}(\gamma_D)\right)^2 d\gamma_D. \end{aligned} \tag{27}$$

Through the substitution of the marginal distribution from (5) and (6) into (27), and further rephrasing the logarithm function and the incomplete Gamma function using Meijer's G-function [38] and the gamma function defined as a series [29], we can ascertain the value of k_2 as

$$\begin{aligned}k_2 &= \left(4\bar{\gamma}_D^{\left(\frac{a_D+1}{2}\right)} b_D^{(a_D+1)}\Gamma(a_D+1)(\Gamma(a_E+1))^2\ln(2)\right)^{-1}\\ &\int_0^\infty \gamma_D^{\frac{a_D-1}{2}} e^{-\frac{1}{b_D}\sqrt{\frac{\gamma_D}{\bar{\gamma}_D}}} G_{2,2}^{1,2}\left(\gamma_D \,|\, {}^{1,1}_{1,0}\right)\\ &\left(G_{1,2}^{1,1}\left(\frac{1}{b_E}\sqrt{\frac{\gamma_D}{\bar{\gamma}_E}} \,|\, {}^{1}_{a_E+1,0}\right)\right)^2 d\gamma_D\\ &= \left(\frac{k_{22}}{2\pi j}\right)\sum_{k=0}^{\infty}\frac{1}{\left(b_E\sqrt{\bar{\gamma}_E}\right)^k\Gamma(a_E+2+k)}\\ &\int_{l_1}\frac{\Gamma(1-s)\Gamma(s)\Gamma(s)}{\Gamma(1+s)}\int_0^\infty \gamma_D^{\frac{a_D+a_E+k+2s}{2}}\\ &e^{-\left(\frac{1}{b_D\sqrt{\bar{\gamma}_D}}+\frac{1}{b_E\sqrt{\bar{\gamma}_E}}\right)\sqrt{\gamma_D}} G_{1,2}^{1,1}\left(\frac{1}{b_E}\sqrt{\frac{\gamma_D}{\bar{\gamma}_E}} \,|\, {}^{1}_{a_E+1,0}\right) d\gamma_D ds\end{aligned} \tag{28}$$

where $k_{22} = (4(b_E\sqrt{\bar{\gamma}_E})^{a_E+1}(b_D\sqrt{\bar{\gamma}_D})^{a_D+1}\Gamma(a_D+1)\Gamma(a_E+1)\ln(2))^{-1}$. Thus, with the help of [37, eq. (2.24.3.1)], the inner integral that define as below can be computed as

$$\begin{aligned}&\int_0^\infty \gamma_D^{\frac{a_D+a_E+k+2s}{2}} e^{-\left(\frac{1}{b_D\sqrt{\bar{\gamma}_D}}+\frac{1}{b_E\sqrt{\bar{\gamma}_E}}\right)\sqrt{\gamma_D}}\\ &G_{1,2}^{1,1}\left(\frac{1}{b_E}\sqrt{\frac{\gamma_D}{\bar{\gamma}_E}} \,|\, {}^{1}_{a_E+1,0}\right) d\gamma_D\\ &= 2\left(\frac{1}{b_D\sqrt{\bar{\gamma}_D}}+\frac{1}{b_E\sqrt{\bar{\gamma}_E}}\right)^{-(a_D+a_E+k+2s+2)}\\ &G_{2,2}^{1,2}\left(\frac{1}{1+\frac{b_E}{b_D}\sqrt{\frac{\bar{\gamma}_E}{\bar{\gamma}_D}}} \,|\, {}^{-(a_D+a_E+k+2s+1),1}_{a_E+1,0}\right).\end{aligned} \tag{29}$$

By plugging (29) into (28), we have

$$\begin{aligned}k_2 &= 2k_{22}\left(\frac{1}{2\pi j}\right)^2\left(\frac{1}{b_D\sqrt{\bar{\gamma}_D}}+\frac{1}{b_E\sqrt{\bar{\gamma}_E}}\right)^{-(a_D+a_E+2)}\\ &\sum_{k=0}^{\infty}\frac{1}{\left(1+\frac{b_E}{b_D}\sqrt{\frac{\bar{\gamma}_E}{\bar{\gamma}_D}}\right)^k\Gamma(a_E+2+k)}\\ &\int_{l_1}\int_{l_2}\left(\frac{1}{b_D\sqrt{\bar{\gamma}_D}}+\frac{1}{b_E\sqrt{\bar{\gamma}_E}}\right)^{-2s}\left(\frac{1}{1+\frac{b_E}{b_D}\sqrt{\frac{\bar{\gamma}_E}{\bar{\gamma}_D}}}\right)^{\xi}\\ &\Gamma(a_D+a_E+k+2s+2+\xi)\\ &\frac{\Gamma(s)\Gamma(s)\Gamma(1-s)\Gamma(a_E+1-\xi)\Gamma(\xi)}{\Gamma(1+s)\Gamma(1+\xi)}d\xi ds.\end{aligned} \tag{30}$$

Hence, through the recognition of the definition of the bivariate Fox H-function [30], k_2 is obtained as

$$k_2 = M_1\sum_{k=0}^{\infty} m_1 H_{1,0:1,2:1,2}^{0,1:1,1:1,1}\left(u_{11}, \eta_{11} \,|\, {}^{\nu_{11}}_{-} \,|\, {}^{\nu_{21}}_{\omega_{21}} \,|\, {}^{\nu_{31}}_{\omega_{31}}\right) \tag{31}$$

where $M_1 = (2(1+[b_D/b_E]\sqrt{[\bar{\gamma}_D/\bar{\gamma}_E]})^{(a_D+1)}(1+[b_E/b_D]\sqrt{[\bar{\gamma}_E/\bar{\gamma}_D]})^{(a_E+1)}\Gamma(a_D+1)\Gamma(a_E+1)\ln(2))^{-1}$, $m_1 = ((1+[b_E/b_D]\sqrt{[\bar{\gamma}_E/\bar{\gamma}_D]})^k\Gamma(a_E+2+k))^{-1}$, $u_{11} = (1/[b_D\sqrt{\bar{\gamma}_D}]+1/[b_E\sqrt{\bar{\gamma}_E}])^{-2}$, $\eta_{11} = (1+[b_E/b_D]\sqrt{[\bar{\gamma}_E/\bar{\gamma}_D]})^{-1}$, $\nu_{11} = (-(1+a_D+a_E+k),2;1)$, $\nu_{21} = (1,1;1)$, $\nu_{31} = (1,1;1)$, $\omega_{21} = (1,1)$, and $\omega_{31} = (a_E+1,1),(0,1;1)$.

Now, for k_3 we have

$$k_3 = \int_0^\infty \log_2(1+\gamma_D) f_{\gamma_D}(\gamma_D) F_{\gamma_D}(\gamma_D) F_{\gamma_E}(\gamma_D) d\gamma_D. \tag{32}$$

In the same way as for k_2, we have

$$k_3 = M_2\sum_{k=0}^{\infty} m_2 H_{1,0:1,2:1,2}^{0,1:1,1:1,1}\left(u_{12}, \eta_{12} \,|\, {}^{\nu_{12}}_{-} \,|\, {}^{\nu_{22}}_{\omega_{22}} \,|\, {}^{\nu_{32}}_{\omega_{32}}\right) \tag{33}$$

where $M_2 = 2M_1$, $m_2 = ((1+[b_D/b_E]\sqrt{[\bar{\gamma}_D/\bar{\gamma}_E]})^k\Gamma(a_D+2+k))^{-1}$, $u_{12} = u_{11}$, $\eta_{12} = (1+[b_D/b_E]\sqrt{[\bar{\gamma}_D/\bar{\gamma}_E]})^{-1}$, $\nu_{12} = \nu_{11}$, $\nu_{22} = \nu_{21}$, $\nu_{32} = \nu_{31}$, $\omega_{22} = \omega_{21}$, and $\omega_{32} = (a_D+1,1),(0,1;1)$. Finally, by inserting (14) into (7) and after some simplification, for the last term in (21), we have

$$k_4 = \frac{1}{2}\int_0^\infty \log_2(1+\gamma_D) f_{\gamma_D}(\gamma_D) F_{\gamma_D}(\gamma_D)\left(F_{\gamma_E}(\gamma_D)\right)^2 d\gamma_D. \tag{34}$$

Next, in a manner analogous to the elucidations provided for the computation of (28), and in accordance with the Cauchy product of two infinite series [29], the value of k_4 can be ascertained as

$$\begin{aligned}k_4 &= k_{44}\sum_{k=0}^{\infty}\left(\frac{{}_2F_1(1,-(k+a_E+1);a_E+2;-1)}{\Gamma(a_E+2)\Gamma(k+a_E+2)}\right.\\ &\left.-\frac{{}_2F_1(1,-a_E;k+a_E+3;-1)}{\Gamma(a_E+1)\Gamma(k+a_E+3)}\right)\left(\frac{1}{b_E\sqrt{\bar{\gamma}_E}}\right)^k\\ &\int_0^\infty \gamma_D^{\frac{a_D+2a_E+1+k}{2}} e^{-\left(\frac{1}{b_D\sqrt{\bar{\gamma}_D}}+\frac{2}{b_E\sqrt{\bar{\gamma}_E}}\right)\sqrt{\gamma_D}}\\ &G_{2,2}^{1,2}\left(\gamma_D \,|\, {}^{1,1}_{1,0}\right) G_{1,2}^{1,1}\left(\frac{1}{b_D}\sqrt{\frac{\gamma_D}{\bar{\gamma}_D}} \,|\, {}^{1}_{a_D+1,0}\right) d\gamma_D\\ &= \left(\frac{k_{44}}{2\pi j}\right)\sum_{k=0}^{\infty}\left(\frac{{}_2F_1(1,-(k+a_E+1);a_E+2;-1)}{\Gamma(a_E+2)\Gamma(k+a_E+2)}\right.\\ &\left.-\frac{{}_2F_1(1,-a_E;k+a_E+3;-1)}{\Gamma(a_E+1)\Gamma(k+a_E+3)}\right)\left(\frac{1}{b_E\sqrt{\bar{\gamma}_E}}\right)^k\\ &\int_{l_1}\frac{\Gamma(1-s)\Gamma(s)\Gamma(s)}{\Gamma(1+s)}\int_0^\infty \gamma_D^{\frac{a_D+2a_E+1+k+2s}{2}}\\ &e^{-\left(\frac{1}{b_D\sqrt{\bar{\gamma}_D}}+\frac{2}{b_E\sqrt{\bar{\gamma}_E}}\right)\sqrt{\gamma_D}} G_{2,2}^{1,2}\left(\gamma_D \,|\, {}^{1,1}_{1,0}\right)\\ &G_{1,2}^{1,1}\left(\frac{1}{b_D}\sqrt{\frac{\gamma_D}{\bar{\gamma}_D}} \,|\, {}^{1}_{a_D+1,0}\right) d\gamma_D ds\end{aligned} \tag{35}$$

where $k_{44} = (4(b_D\sqrt{\bar{\gamma}_D})^{(a_D+1)}(b_E\sqrt{\bar{\gamma}_E})^{2(a_E+1)}(\Gamma(a_D+1))^2\ln(2))^{-1}$. Thus, with the help of [38, eq. (24.3.1)], and after computing the inner integral and some simplification, k_4 can be computed as follows:

$$\begin{aligned}k_4 &= 2k_{44}\left(\frac{1}{2\pi j}\right)^2\left(\frac{1}{b_D\sqrt{\bar{\gamma}_D}}+\frac{2}{b_E\sqrt{\bar{\gamma}_E}}\right)^{-(a_D+2a_E+3)}\\ &\sum_{k=0}^{\infty}\left(2+\frac{b_E\sqrt{\bar{\gamma}_E}}{b_D\sqrt{\bar{\gamma}_D}}\right)^{-k}\left(\frac{{}_2F_1(1,-(k+a_E+1);a_E+2;-1)}{\Gamma(a_E+2)\Gamma(k+a_E+2)}\right.\end{aligned}$$

$$- \frac{{}_2F_1(1, -a_E; k + a_E + 3; -1)}{\Gamma(a_E + 1)\Gamma(k + a_E + 3)}\Bigg)$$
$$\int_{l_1}\int_{l_2}\left(\frac{1}{b_D\sqrt{\bar{\gamma}_D}} + \frac{2}{b_E\sqrt{\bar{\gamma}_E}}\right)^{-2s}\left(\frac{1}{1 + 2\frac{b_D}{b_E}\sqrt{\frac{\bar{\gamma}_D}{\bar{\gamma}_E}}}\right)^{\xi}$$
$$\frac{\Gamma(a_D + 2a_E + k + 2s + 2 + \xi)}{\Gamma(1 + s)\Gamma(1 + \xi)}\frac{\Gamma(s)\Gamma(s)\Gamma(1 - s)\Gamma(a_D + 1 - \xi)\Gamma(\xi)}{\Gamma(1 + s)\Gamma(1 + \xi)}d\xi ds \tag{36}$$

Hence, through the recognition of the definition of bivariate Fox H-function [30], k_4 is derived as

$$k_4 = M_3\sum_{k=0}^{\infty} m_3 H^{0,1:1,2:1,1}_{1,0:2,2:1,2}\left(u_{13}, \eta_{13} \,|\, {}^{\nu_{13}}_{-} \,|\, {}^{\nu_{23}}_{\omega_{23}} \,|\, {}^{\nu_{33}}_{\omega_{33}}\right) \tag{37}$$

where $M_3 = (2(1 + 2[b_D/b_E]\sqrt{[\bar{\gamma}_D/\bar{\gamma}_E]})^{(a_D+1)}(1 + 2[b_E/b_D]\sqrt{[\bar{\gamma}_E/\bar{\gamma}_D]})^{2(a_E+1)}(\Gamma(a_D + 1))^2\ln(2))^{-1}$, $m_3 = ([{}_2F_1(1, -(k + a_E + 1); a_E + 2; -1)]/[\Gamma(a_E + 2)\Gamma(k + a_E + 2)] - [{}_2F_1(1, -a_E; k + a_E + 3; -1)]/[\Gamma(a_E + 1)\Gamma(k + a_E + 3)])(2 + [b_E]/[b_D]\sqrt{[\bar{\gamma}_E/\bar{\gamma}_D]})^{-k}$, $u_{13} = u_{11}$, $\eta_{13} = (1 + 2[b_D/b_E]\sqrt{[\bar{\gamma}_D/\bar{\gamma}_E]})^{-1}$, $\nu_{13} = (-(1 + a_D + 2a_E + k), 2; 1)$, $\nu_{23} = (1, 1; 1), (1, 1; 1)$, $\nu_{33} = (1, 1; 1)$, $\omega_{23} = (1, 1)$, and $\omega_{33} = (a_D + 1, 1), (0, 1; 1)$.

Similarly, for the terms in (22), we have

$$A_1 = \int_0^{\infty}\log_2(1 + \gamma_E)f_{\gamma_E}(\gamma_E)\big(1 - F_{\gamma_D}(\gamma_E)\big)d\gamma_E \tag{38}$$
$$A_2 = \int_0^{\infty}\log_2(1 + \gamma_E)f_{\gamma_E}(\gamma_E)F_{\gamma_E}(\gamma_E)\big(1 - F_{\gamma_D}(\gamma_E)\big)d\gamma_E \tag{39}$$
$$A_3 = \frac{1}{2}\int_0^{\infty}\log_2(1 + \gamma_E)f_{\gamma_E}(\gamma_E)\Big(1 - (F_{\gamma_D}(\gamma_E))^2\Big)d\gamma_E \tag{40}$$

and

$$A_4 = \frac{1}{2}\int_0^{\infty}\log_2(1 + \gamma_E)f_{\gamma_E}(\gamma_E)F_{\gamma_D}(\gamma_E)\Big(1 - (F_{\gamma_D}(\gamma_E))^2\Big)d\gamma_E. \tag{41}$$

The approach for solving these integrals is analogous to the methodology used in the initial part of this proof, hence we abstain from providing the detailed derivations here. After appropriate simplification, these integrals allow us to express (7) in closed-form by inserting (26), (31), (33), (37), and (38)–(41) in (20). This completes the proof.

Appendix B
Proof of Theorem 3

By inserting (8) and (14) into SOP definition, P_{sop} is expressed as

$$P_{\text{sop}} = P_1 + \theta(P_1 - 2P_2 - 2P_3 + 4P_4) \tag{42}$$

where

$$P_1 = \int_0^{\infty}F_{\gamma_D}(\gamma_t)f_{\gamma_E}(\gamma_E)d\gamma_E \tag{43}$$
$$P_2 = \int_0^{\infty}F_{\gamma_D}(\gamma_t)f_{\gamma_E}(\gamma_E)F_{\gamma_E}(\gamma_E)d\gamma_E \tag{44}$$
$$P_3 = \frac{1}{2}\int_0^{\infty}\big(F_{\gamma_D}(\gamma_t)\big)^2 f_{\gamma_E}(\gamma_E)d\gamma_E \tag{45}$$

and

$$P_4 = \frac{1}{2}\int_0^{\infty}\big(F_{\gamma_D}(\gamma_t)\big)^2 f_{\gamma_E}(\gamma_E)F_{\gamma_E}(\gamma_E)d\gamma_E. \tag{46}$$

For the first term in (42), we have

$$P_1 = \int_0^{\infty}F_{\gamma_D}(\gamma_t)f_{\gamma_E}(\gamma_E)d\gamma_E \tag{47}$$

where $\gamma_t = (1 + \gamma_E)2^{R_s} - 1$.

Through the application of the Parseval relation relevant in the Mellin transform [4], [29], (43) can be reformulated as

$$P_1 = \frac{1}{2\pi i}\int_{l_1}M[F_{\gamma_D}(\gamma_t), 1 - s]M[f_{\gamma_E}(\gamma_E), s]ds \tag{48}$$

where l_1 refers to the integration path from $v - j\infty$ to $v + j\infty$ for a fixed value of v. Next, by applying the definition of Meijer's G-function, we can express $M[F_{\gamma_D}((1 + \gamma_E)2^{R_s} - 1), 1 - s]$ as:

$$\begin{aligned}M[F_{\gamma_D}(\gamma_t), 1 - s] &= \int_0^{\infty}\gamma_E^{-s}F_{\gamma_D}(\gamma_t)d\gamma_E\\ &= \frac{1}{\Gamma(a_D + 1)}\int_0^{\infty}\gamma_E^{-s}G^{1,1}_{1,2}\left(\frac{1}{b_D}\sqrt{\frac{\gamma_t}{\bar{\gamma}_D}}\,\middle|\,{}^{1}_{a_D+1,0}\right)d\gamma_E\\ &= \frac{1}{2\pi i\Gamma(a_D + 1)}\int_{l_2}\int_0^{\infty}\gamma_E^{-s}\left(\frac{1}{b_D}\sqrt{\frac{\gamma_t}{\bar{\gamma}_D}}\right)^{-\xi}\\ &\quad\frac{\Gamma(a_D + 1 + \xi)\Gamma(-\xi)}{\Gamma(1 - \xi)}d\gamma_E d\xi\end{aligned} \tag{49}$$

where the last equality is obtained by utilizing the definition of Meijer's G-function and interchanging the order of integration. By employing the methods outlined in [29, eq. (3.194.3)], the inner integral in (49) can be evaluated as:

$$\begin{aligned}\int_0^{\infty}\gamma_E^{-s}\gamma_t^{-\frac{\xi}{2}}d\gamma_E &= \int_0^{\infty}\gamma_E^{-s}\big((1 + \gamma_E)2^{R_s} - 1\big)^{-\frac{\xi}{2}}d\gamma_E\\ &= \big(2^{R_s} - 1\big)^{-\frac{\xi}{2}}\left(1 + \frac{1}{2^{R_s} - 1}\right)^{s-1}B\left(1 - s, \frac{\xi}{2} + s - 1\right)\\ &= \big(2^{R_s} - 1\big)^{-\frac{\xi}{2}}\left(1 + \frac{1}{2^{R_s} - 1}\right)^{s-1}\frac{\Gamma(1 - s)\Gamma\left(\frac{\xi}{2} + s - 1\right)}{\Gamma\left(\frac{\xi}{2}\right)}\end{aligned} \tag{50}$$

where (50) is obtained by representing $\gamma_t = (1 + \gamma_E)2^{R_s} - 1$, and last equality is obtained by utilizing the property of beta function where $B(a_1, b_1) = (\Gamma(a_1)\Gamma(b_1))/(\Gamma(a_1 + b_1))$. Now, by inserting (50) into (49), we have:

$$\begin{aligned}M[F_{\gamma_D}(\gamma_t), 1 - s] &= \frac{\Gamma(1 - s)}{2\pi i\Gamma(a_D + 1)}\left(1 + \frac{1}{2^{R_s} - 1}\right)^{s-1}\\ &\int_{l_2}\frac{\Gamma(a_D + 1 + \xi)\Gamma(-\xi)\Gamma(\frac{\xi}{2} + s - 1)}{\Gamma(\frac{\xi}{2})\Gamma(1 - \xi)}\left(b_D\sqrt{\frac{\bar{\gamma}_D}{2^{R_s} - 1}}\right)^{\xi}d\xi,\end{aligned} \tag{51}$$

where l_2 is a specific counter. Next, with the aid of [39, eq. (2.9)], the Mellin transform $M[f_{\gamma_E}(\gamma_E), s]$ is given by

$$\begin{aligned}M[f_{\gamma_E}(\gamma_E), s] &= \int_0^{\infty}\gamma_E^{(s-1)}f_{\gamma_E}(\gamma_E)d\gamma_E\\ &= \frac{1}{2\bar{\gamma}_E^{(\frac{a_E+1}{2})}b_E^{(a_E+1)}\Gamma(a_E + 1)}\int_0^{\infty}\gamma_E^{(\frac{a_E-3+2s}{2})}e^{-\frac{1}{b_E}\sqrt{\frac{\gamma_E}{\bar{\gamma}_E}}}d\gamma_E\end{aligned}$$

$$= \frac{(b_E\sqrt{\bar{\gamma}_E})^{2(s-1)}\Gamma(a_E-1+2s)}{\Gamma(a_E+1)}. \quad (52)$$

Then, by substituting (51) and (52) into (48), P_1 can be written as

$$P_1 = \left(\frac{1}{2\pi i}\right)^2\left(1-\frac{1}{2^{R_s}}\right)(\frac{1}{b_E\sqrt{\bar{\gamma}_E}})^2\frac{1}{\Gamma(a_D+1)\Gamma(a_E+1)}$$
$$\int_{l_1}\int_{l_2}\left(b_E^2\bar{\gamma}_E\left(1+\frac{1}{2^{R_s}-1}\right)\right)^s\left(b_D\sqrt{\frac{\bar{\gamma}_D}{2^{R_s}-1}}\right)^{\xi}\Gamma\left(\frac{\xi}{2}+s-1\right)$$
$$\frac{\Gamma(1-s)\Gamma(a_E-1+2s)\Gamma(a_D+1+\xi)\Gamma(-\xi)}{\Gamma\left(\frac{\xi}{2}\right)\Gamma(1-\xi)}d\xi ds. \quad (53)$$

Through the application of the Parseval relation relevant in the Mellin transform [4], [29], (44) can be rewritten as follows:

$$P_2 = \frac{1}{2\pi i}\int_{l_1} M\left[F_{\gamma_D}(\gamma_t), 1-s\right]M\left[f_{\gamma_E}(\gamma_E)F_{\gamma_E}(\gamma_E), s\right]ds. \quad (54)$$

Then, similar to (49), $M[F_{\gamma_D}(\gamma_t), 1-s]$ can be obtained as

$$M\left[F_{\gamma_D}(\gamma_t), 1-s\right] = \frac{\Gamma(1-s)}{2\pi i\Gamma(a_D+1)}\left(1+\frac{1}{2^{R_s}-1}\right)^{s-1}$$
$$\int_{l_2}\frac{\Gamma(a_D+1+\xi)\Gamma(-\xi)\Gamma(\frac{\xi}{2}+s-1)}{\Gamma(\frac{\xi}{2})\Gamma(1-\xi)}(b_D\sqrt{\frac{\bar{\gamma}_D}{2^{R_s}-1}})^{\xi}d\xi \quad (55)$$

where l_2 is a specific counter. Next, with the aid of [39, eq. (2.9)], the Mellin transform $M[f_{\gamma_E}(\gamma_E)F_{\gamma_E}(\gamma_E), s]$ is given by

$$M\left[f_{\gamma_E}(\gamma_E)F_{\gamma_E}(\gamma_E), s\right] = \int_0^{\infty}\gamma_E^{(s-1)}f_{\gamma_E}(\gamma_E)F_{\gamma_E}(\gamma_E)d\gamma_E$$
$$= \frac{1}{2\bar{\gamma}_E^{\left(\frac{a_E+1}{2}\right)}b_E^{(a_E+1)}(\Gamma(a_E+1))^2}\int_0^{\infty}\gamma_E^{\left(\frac{a_E-3+2s}{2}\right)}e^{-\frac{1}{b_E}\sqrt{\frac{\gamma_E}{\bar{\gamma}_E}}}$$
$$G_{1,2}^{1,1}\left(\frac{1}{b_E}\sqrt{\frac{\gamma_E}{\bar{\gamma}_E}}\,|\,{}^{1}_{a_E+1,0}\right)d\gamma_E = \frac{1}{(\Gamma(a_E+1))^2}$$
$$\left(b_E\sqrt{\bar{\gamma}_E}\right)^{2(s-1)}G_{2,2}^{1,2}\left(1\,|\,{}^{-(a_E+2s-2),1}_{a_E+1,0}\right) \quad (56)$$

Then, by substituting (55) and (56) in (54), P_2 can be written as

$$P_2 = \left(\frac{1}{2\pi i}\right)^2\left(1-\frac{1}{2^{R_s}}\right)\left(\frac{1}{b_E\sqrt{\bar{\gamma}_E}}\right)^2\frac{1}{\Gamma(a_D+1)(\Gamma(a_E+1))^2}$$
$$\int_{l_1}\int_{l_2}\left(b_E^2\bar{\gamma}_E(1+\frac{1}{2^{R_s}-1})\right)^s\left(b_D\sqrt{\frac{\bar{\gamma}_D}{2^{R_s}-1}}\right)^{\xi}\Gamma\left(\frac{\xi}{2}+s-1\right)$$
$$\frac{\Gamma(1-s)\Gamma(a_E-1+2s)\Gamma(a_D+1+\xi)\Gamma(-\xi)}{\Gamma\left(\frac{\xi}{2}\right)\Gamma(1-\xi)}d\xi ds. \quad (57)$$

By similar manner P_3 and P_4 can be computed as follows:

$$P_3 = \frac{\left(1-2^{R_s}\right)^{(a_D+2)}}{\sqrt{\pi}\Gamma(a_E+1)\left(b_E\sqrt{\bar{\gamma}_E}\right)^2\left(b_D\sqrt{\bar{\gamma}_D}\right)^{2(a_D+1)}2^{(1+R_s)}}$$
$$\sum_{k=0}^{\infty}\sum_{k'=0}^{\infty}\frac{\left(1-2^{R_s}\right)^{\frac{k+k'}{2}}}{\left(b_D\sqrt{\bar{\gamma}_D}\right)^{k+k'}\Gamma(a_D+2+k)\Gamma(a_D+2+k')}$$
$$\int_{l_1}\int_{l_2}\left(\left(\frac{1}{1-2^{R_s}}-1\right)(b_E\sqrt{\bar{\gamma}_E}\right)^2\right)^s\left(b_D\sqrt{\frac{\bar{\gamma}_D}{2^{R_s}-1}}\right)^{\xi}$$
$$\Gamma\left(-(a_D+2+\frac{k+k'}{2}-s+\xi)\right)\Gamma(a_E-1+2s)$$
$$\frac{\Gamma\left(a_D+2+\frac{k+k'}{2}+\xi\right)\Gamma(-\xi)\Gamma\left(\frac{1}{2}-\xi\right)}{\Gamma(s)\Gamma(1+\xi)\Gamma\left(\frac{1}{2}+\xi\right)}d\xi ds \quad (58)$$

and

$$P_4 = \frac{\left(1-2^{R_s}\right)^{(a_D+2)}}{\sqrt{\pi}(\Gamma(a_E+1))^2\left(b_E\sqrt{\bar{\gamma}_E}\right)^2\left(b_D\sqrt{\bar{\gamma}_D}\right)^{2(a_D+1)}2^{(1+R_s)}}$$
$$\sum_{k=0}^{\infty}\sum_{k'=0}^{\infty}\frac{\left(1-2^{R_s}\right)^{\frac{k+k'}{2}}}{\left(b_D\sqrt{\bar{\gamma}_D}\right)^{k+k'}\Gamma(a_D+2+k)\Gamma(a_D+2+k')}$$
$$\int_{l_1}\int_{l_2}\left((\frac{1}{1-2^{R_s}}-1)(b_E\sqrt{\bar{\gamma}_E})^2\right)^s\left(b_D\sqrt{\frac{\bar{\gamma}_D}{2^{R_s}-1}}\right)^{\xi}$$
$$\Gamma\left(-(a_D+2+\frac{k+k'}{2}-s+\xi)\right)\Gamma(a_E-1+2s)\Gamma(1-s)$$
$$\frac{\Gamma\left(a_D+2+\frac{k+k'}{2}+\xi\right)\Gamma(-\xi)\Gamma\left(\frac{1}{2}-\xi\right)}{\Gamma(s)\Gamma(1+\xi)\Gamma\left(\frac{1}{2}+\xi\right)}d\xi ds. \quad (59)$$

Eventually, the proof is accomplished by leveraging the representation of bivariate Fox H-function through a double contour integral [30] and inserting (53), (57), (58), and (59) into (42), the proof is completed.

Appendix C
Proof of Theorem 4

In the scenario where $\bar{\gamma}_D$ approaches infinity, the ASC can be defined as

$$\bar{C}_s^{\,asy} = J_1' - J_2' \quad (60)$$

where

$$J_1' = k_1' + \theta(k_1' - 2k_2' - 2k_3' + 4k_4') \quad (61)$$

and

$$J_2' = A_1' + \theta(A_1' - 2A_2' - 2A_3' + 4A_4'). \quad (62)$$

For the first term in (61), by considering (21), we can find the value of k_1' by evaluating the bivariate Fox's H-function as defined in (25) at the highest poles on the left side of l_2. These poles occur at $s=0$ and $s=-(1+a_D+\xi)/2$ on the left of contour l_1. Thus, by using the residue theorem [4], [32], we have

$$C_1 = \frac{1}{2\pi i}\int_{l_1}\frac{\Gamma(1+a_D+2S+\xi)\Gamma(1-s)\Gamma(s)\Gamma(s)}{\Gamma(1+s)}\left(b_D^2\bar{\gamma}_D\right)^s ds$$
$$= \mathrm{Res}\left[\frac{\Gamma(1-s)\Gamma(s)\Gamma(s)\left(b_D^2\bar{\gamma}_D\right)^s}{\Gamma(1+s)}, -\frac{1+a_D+\xi}{2}\right]$$
$$+\mathrm{Res}\left[\frac{\Gamma(1-s)\Gamma^2(s)\left(b_D^2\bar{\gamma}_D\right)^s}{\Gamma(1+s)}, 0\right]$$
$$= \lim_{s\to-\frac{1+a_D+\xi}{2}}\left(s+\frac{1+a_D+\xi}{2}\right)$$
$$\frac{\Gamma(1-s)\Gamma^2(s)\left(b_D^2\bar{\gamma}_D\right)^s}{\Gamma(1+s)}+\Gamma(1+a_D+\xi) = \left(b_D\sqrt{\bar{\gamma}_D}\right)^{-(1+a_D+\xi)}$$

$$\frac{\Gamma\left(\frac{3+a_D+\xi}{2}\right)-\Gamma^2\left(-\frac{1+a_D+\xi}{2}\right)}{\Gamma\left(\frac{1-a_D-\xi}{2}\right)}+\Gamma(1+a_D+\xi). \tag{63}$$

Now, by inserting (63) into (25) and subsequently calculating the rightmost pole above the contour labeled as l_2, specifically denoted as $\xi = a_E + 1$, we obtain the following result:

$$k_1' = \frac{(b_D\sqrt{\bar{\gamma}_D})^{-(a_D+1)}(b_E\sqrt{\bar{\gamma}_E})^{-(a_E+1)}}{\ln(2)\Gamma(a_D+1)\Gamma(a_E+2)}(\Gamma(a_D+a_E+2) + \frac{\Gamma\left(\frac{a_D+a_E+4}{2}\right)\Gamma^2\left(-\frac{a_D+a_E+2}{2}\right)}{\Gamma\left(-\frac{a_D+a_E}{2}\right)}\left(b_E\sqrt{\bar{\gamma}_E}\right)^{-(a_E+a_D+2)}\Big). \tag{64}$$

In a similar manner, we can determine the remaining parameters in (61) and (62) by employing the residue theorem. This completes the proof.

Appendix D
Proof of Theorem 5

In the scenario where $\bar{\gamma}_D$ approaches infinity, the bivariate Fox's H-function in the first term of (17) is evaluated at its most prominent poles to the left of l_2, which occur when $\xi = 2(1-s)$. Consequently, we derive the following outcomes for the counter l_2:

$$\begin{aligned} R_2 &= \frac{1}{2\pi i}\int_{l_2}\frac{\Gamma(a_D+1+\xi)\Gamma(-\xi)\left(b_D\sqrt{\frac{\bar{\gamma}_D}{2^{R_s}-1}}\right)^{\xi}}{\Gamma\left(\frac{\xi}{2}\right)\Gamma(1-\xi)}\Gamma\left(\frac{\xi}{2}+s-1\right)d\xi \\ &= \mathrm{Res}\left[\frac{\Gamma(a_D+1+\xi)\Gamma(-\xi)\left(b_D\sqrt{\frac{\bar{\gamma}_D}{2^{R_s}-1}}\right)^{\xi}}{\Gamma\left(\frac{\xi}{2}\right)\Gamma(1-\xi)}, 2(1-s)\right] = \\ &\lim_{\xi\to 2(1-s)}\left(\frac{\xi}{2}+s-1\right)\frac{\Gamma(a_D+1+\xi)\Gamma(-\xi)\left(b_D\sqrt{\frac{\bar{\gamma}_D}{2^{R_s}-1}}\right)^{\xi}}{\Gamma\left(\frac{\xi}{2}\right)\Gamma(1-\xi)} \\ &= \frac{\Gamma(a_D+3-2s)\Gamma(2s-2)}{\Gamma(1-s)\Gamma(2s-1)}\left(b_D\sqrt{\frac{\bar{\gamma}_D}{2^{R_s}-1}}\right)^{2(1-s)}. \end{aligned} \tag{65}$$

Subsequently, through the application of (65) to (17), the first term of the asymptotic SOP can be established as follows:

$$P_{1,\mathrm{sop}}^{\mathrm{asy}} = \left(\frac{1}{2\pi i}\right)\left(\frac{1}{2^{R_s}}\right)\left(\frac{b_D}{b_E}\sqrt{\frac{\bar{\gamma}_D}{\bar{\gamma}_E}}\right)^2\frac{1}{\Gamma(a_D+1)\Gamma(a_E+1)} \int_{l_1}\frac{\Gamma(a_D+3-2s)\Gamma(2s-2)\Gamma(a_E-1+2s)}{\Gamma(2s-1)\left(\frac{b_D{}^2\bar{\gamma}_D}{b_E{}^2\bar{\gamma}_E 2^{R_s}}\right)^s}ds. \tag{66}$$

Subsequently, through the determination of the rightmost highest pole along contour l_1, which corresponds to $s = (a_D+3)/2$, (66) can be simplified to its asymptotic form. The asymptotic behavior of the other terms in (17) can be derived similarly as expressed in (19), thus concluding the proof.

References

[1] E. Basar, M. Di Renzo, J. De Rosny, M. Debbah, M. S. Alouini, and R. Zhang, "Wireless communications through reconfigurable intelligent surfaces," *IEEE Access*, vol. 7, pp. 116753–116773, 2019.

[2] A. D. Wyner, "The wire-tap channel," *Bell Syst. Tech. J.*, vol. 54, no. 8, pp. 1355–1387, Oct. 1975.

[3] S. K. Yoo, S. L. Cotton, P. C. Sofotasios, M. Matthaiou, M. Valkama, and G. K. Karagiannidis, "The fisher–snedecor $\mathcal{F}$ distribution: A simple and accurate composite fading model," *IEEE Commun. Lett.*, vol. 21, no. 7, pp. 1661–1664, Jul. 2017.

[4] L. Kong, "Wireless networks physical layer security: modeling and performance characterization." Ph.D. dissertation, École de Technologie Supérieure, Aug. 2019.

[5] N. Mensi and D. B. Rawat, "PLS of NOMA relaying networks under Fisher-Snedecor $\mathcal{F}$ composite fading," in *Proc. IEEE ICC*, May 2023, pp. 4515–4520.

[6] G. Li, M. Zeng, D. Mishra, L. Hao, Z. Ma, and O. A. Dobre, "Latency minimization for IRS-aided NOMA MEC systems with WPT-enabled IoT devices," *IEEE Internet Things J.*, vol. 10, no. 14, pp. 12156–12168, Jul. 2023.

[7] Z. Xie et al., "Resource allocation for double IRSs assisted wireless powered NOMA networks," *IEEE Wireless Commun. Lett.*, vol. 12, no. 5, pp. 823–827, May 2023.

[8] W. Hao, F. Zhou, M. Zeng, O. A. Dobre, and N. Al-Dhahir, "Ultra wideband THz IRS communications: Applications, challenges, key techniques, and research opportunities," *IEEE Netw.*, vol. 36, no. 6, pp. 214–220, Nov./Dec. 2022.

[9] W. Hao, J. Li, G. Sun, M. Zeng, and O. A. Dobre, "Securing reconfigurable intelligent surface-aided cell-free networks," *IEEE Trans. Inf. Forensics Security*, vol. 17, pp. 3720–3733, 2022.

[10] X. Li, Y. Zheng, M. Zeng, Y. Liu, and O. A. Dobre, "Enhancing secrecy performance for STAR-RIS NOMA networks," *IEEE Trans. Veh. Technol.*, vol. 72, no. 2, pp. 2684–2688, Oct. 2022.

[11] L. Yang, J. Yang, W. Xie, M. O. Hasna, T. Tsiftsis, and M. Di Renzo, "Secrecy performance analysis of RIS-aided wireless communication systems," *IEEE Trans. Veh. Technol.*, vol. 69, no. 10, pp. 12296–12300, Oct. 2020.

[12] A. K. Yadav, S. Yadav, A. Pandey, and A. Silva, "On the secrecy performance of RIS-enabled wireless communications over Nakagami-m fading channels," *ICT Exp.*, vol. 9, no. 3, pp. 452–458, Jun. 2023.

[13] A. Makarfi, K. Rabie, O. Kaiwartya, O. Badarneh, G. Nauryzbayev, and R. Kharel, "Physical layer security in RIS-assisted networks in Fisher-Snedecor composite fading," in *Proc. Int. Symp. Commun. Syst., Netw. Digital Signal Process. (CSNDSP)*, 2020, pp. 1–6.

[14] J. Zhang, H. Du, Q. Sun, B. Ai, and D. W. K. Ng, "Physical layer security enhancement with reconfigurable intelligent surface-aided networks," *IEEE Trans. Inf. Forensics Security*, vol. 16, pp. 3480–3495, 2021.

[15] F. R. Ghadi, W. P. Zhu, and D. Martín, "RIS-aided secure communications over Fisher-Snedecor F fading channels," Aug. 2022, *arXiv:2208.07274*.

[16] F. R. Ghadi, W. P. Zhu, and D. Martín, "RIS-aided secure communications over Fisher-Snedecor F fading channels," Apr. 2023, *arXiv:2208.07274*.

[17] D.-S. Shiu, G. J. Foschini, M. J. Gans, and J. M. Kahn, "Fading correlation and its effect on the capacity of multielement antenna systems," *IEEE Trans. Commun.*, vol. 48, no. 3, pp. 502–513, Mar. 2000.

[18] R. B. Nelsen, *An Introduction to Copulas*, New York, NY, USA: Springer, Jun. 2007.

[19] P. Kumar, "Copula functions and applications in engineering," in *Logistics, Supply Chain and Financial Predictive Analytics: Theory and Practices*, Singapore: Springer, 2019, pp. 195–209.

[20] E. A. Jorswieck and K.-L. Besser, "Copula-based bounds for multi-user communications—Part I: Average Performance," *IEEE Commun. Lett.*, vol. 25, no. 1, pp. 3–7, Jan. 2021.

[21] K.-L. Besser and E. A. Jorswieck, "Copula-based bounds for multi-user communications—Part II: Outage performance," *IEEE Commun. Lett.*, vol. 25, no. 1, pp. 8–12, Jan. 2021.

[22] K.-L. Besser and E. A. Jorswieck, "Bounds on the secrecy outage probability for dependent fading channels," *IEEE Trans. Commun.*, vol. 69, no. 1, pp. 443–456, Jan. 2021.

[23] S. Pakravan and G. A. Hodtani, "Copula based analysis of impact of wireless channels correlation on the physical layer security performances in a wireless wiretap channel with artificial noise," *Trans. Emerg. Telecommun. Technol.*, vol. 33, no. 4, Apr. 2022, Art. no. e4436.

[24] F. R. Ghadi and W.-P. Zhu, "Performance analysis over correlated/independent fisher-snedecor $\mathcal{F}$ fading multiple access channels," *IEEE Trans. Veh. Technol.*, vol. 71, no. 7, pp. 7561–7571, Jul. 2022.

[25] K.-L. Besser and E. A. Jorswieck, "Calculation of bounds on the ergodic capacity for fading channels with dependency uncertainty," in *Proc. IEEE Int. Conf. Commun.*, 2021, pp. 1–6,

[26] S. A. Mohajeran and G. A. Hodtani, "Copula-based analysis of power allocation for two-sensor composite fading MAC with dependent channel coefficients," *IEEE Syst. J.*, vol. 15, no. 3, pp. 4240–4247, Sep. 2021.

[27] K.-L. Besser, P.-H. Lin, and E. A. Jorswieck, "On fading channel dependency structures with a positive zero-outage capacity," *IEEE Trans. Commun.*, vol. 69, no. 10, pp. 6561–6574, Oct. 2021.
[28] C. Zheng, M. Egan, L. Clavier, G. W. Peters, and J.-M. Gorce, "Copula-based interference models for IoT wireless networks," in *Proc. IEEE Int. Conf. Commun. (ICC)*, 2019, pp. 1–6,
[29] D. Zwillinger and J. Alan, *Table of Integrals, Series, and Products*. Amsterdam, The Netherlands: Elsevier, 2007.
[30] A. M. Mathai, R. K. Saxena, and H. J. Haubold, *The H-Function: Theory and Applications*. Berlin, Germany: Springer, 2009.
[31] S. Sriboonchitta and V. Kreinovich, "Why are FGM copulas successful? A simple explanation," *Adv. Fuzzy Syst.*, vol. 2018, May 2018, Art. no. 5872195.
[32] H. Chergui, M. Benjillali, and S. Saoudi, "Performance analysis of project-and-forward relaying in mixed MIMO-pinhole and Rayleigh dual-hop channel," *IEEE Commun. Lett.*, vol. 20, no. 3, pp. 610–613, Mar. 2016.
[33] K. O. Odeyemi, P. A. Owolawi, and O. O. Olakanmi, "Reconfigurable intelligent surface assisted mobile network with randomly moving user over fisher-snedecor fading channel," *Phys. Commun.*, vol. 43, Dec. 2020, Art. no. 101186.
[34] A. U. Makarfi, K. M. Rabie, O. Kaiwartya, O. S. Badarneh, X. Li, and R. Kharel, "Reconfigurable intelligent surface enabled IoT networks in generalized fading channels," in *Proc. ICC IEEE Int. Conf. Commun. (ICC)*, 2020, pp. 1–6.
[35] L. Kong and G. Kaddoum, "On physical layer security over the Fisher-Snedecor $\mathcal{F}$ wiretap fading channels," *IEEE Access*, vol. 6, pp. 39466–39472, 2018.
[36] K. P. Peppas, "A new formula for the average bit error probability of dual-hop amplify-and-forward relaying systems over generalized shadowed fading channels," *IEEE Wireless Commun. Lett.*, vol. 1, no. 2, pp. 85–88, Apr. 2012.
[37] M. Coblenz, "MATVines: A vine copula package for MATLAB," *SoftwareX*, vol. 14, Jun. 2021, Art. no. 100700. [Online]. Available: https://www.sciencedirect.com/science/article/pii/S2352711021000455
[38] O. S. Badarneh, P. C. Sofotasios, S. Muhaidat, S. L. Cotton, and D. B. Da Costa, "Product and ratio of product of fisher-snedecor $\mathcal{F}$ variates and their applications to performance evaluations of wireless communication systems," *IEEE Access*, vol. 8, pp. 215267–215286, 2020.
[39] A. Prudnikov, Y. A. Brychkov, and O. Marichev, *Integrals and Series: More Special Functions*. vol. 3. London, U.K.: Gordon and Breach, 1990.